Received: 13 July 2022 | Revised: 15 September 2022 | Accepted: 21 September 2022

DOI: 10.1002/ecs2.4449

ARTICLE

ECOSPHERE
AN ESA OPEN ACCESS JOURNAL

Spatial Bayesian models project shifts in suitable habitat for Pacific Northwest tree species under climate change

Karin Kralicek[1,2] | **Jay M. Ver Hoef**[3] | **Tara M. Barrett**[4] | **Hailemariam Temesgen**[2]

[1]Forest Inventory and Analysis Program, Rocky Mountain Research Station, USDA Forest Service, Fort Collins, Colorado, USA

[2]Forest Measurements and Biometrics Laboratory, Department of Forest Engineering, Resources, and Management, Oregon State University, Corvallis, Oregon, USA

[3]Marine Mammal Laboratory, Alaska Fisheries Science Center, NOAA National Marine Fisheries Service, Seattle, Washington, USA

[4]Pacific Northwest Research Station, USDA Forest Service, Wenatchee, Washington, USA

Correspondence
Karin Kralicek
Email: karin.kralicek@usda.gov

Funding information
U.S. Department of Agriculture, Forest Service; Oak Ridge Institute for Science and Education (ORISE)

Handling Editor: Debra P. C. Peters

Abstract

We developed spatial Bayesian hierarchical models to assess potential climate change impacts on suitable habitat for five important tree species in the Pacific northwestern United States (California, Oregon, and Washington). Individual-species models were fit with presence–absence data from forest inventory field plots and spatial relationships were specified through a conditional autoregressive model. This modeling approach allowed us to visualize uncertainty in response curves, map current and future prediction uncertainty, and provide interval estimates for change. Upward elevational or northward latitudinal shifts in climatically suitable habitat were projected for all species. Climate change impacts were the most damaging for noble fir (*Abies procera*), for which 79%–100% of the current range was projected to become climatically unsuitable by the 2080s. Although coastal Douglas-fir (*Pseudotsuga menziesii* var. *menziesii*) has been projected by others to gain habitat in Canada, within our study area we projected a net loss of climatically suitable habitat (ca. 8000–31,400 km^2) under three of four future climate scenarios. A net loss in habitat was also projected for Oregon white oak (*Quercus garryana*) under three of four scenarios, with 40%–60% of the current range becoming unsuitable. Although there was no net loss of habitat for forest land blue oak under any scenario, other factors like competition may inhibit blue oak (*Quercus douglasii*) and white oak from occupying areas projected to increase in climatic suitability. Additionally, between 13% and 32% of blue oak's current range was projected to become unsuitable; some of these areas aligned with dieback following the 2012–2015 California drought, which our data set predates. Unlike the other four species, we projected a 17%–25% increase in climatically suitable habitat for California black oak (*Quercus kelloggii*), although 1%–20% of the current range was still projected to become unsuitable. Our findings indicate that, although some species will face more pressure in tracking climatically suitable habitat than others, climate change will impact the location of suitable habitat for many species.

KEYWORDS
Bayesian hierarchical model, climate change, conditional autoregressive, forest inventory and analysis, habitat suitability, species distribution models, species range, species response curves, tree species

INTRODUCTION

Rapid changes to climate are impacting and will continue to impact the location of suitable habitat for many tree species (Lenoir et al., 2008; Mathys et al., 2017; McKenney et al., 2007; Soja et al., 2007). Within this century, warmer temperatures and changes to the timing and amount of precipitation are projected for the Pacific Northwest (PNW) region of the contiguous United States (Garfin et al., 2014; Mote et al., 2014). In response to climate change, the geographic ranges of many tree species in North America are expected to move upward in elevation and northward in latitude (Iverson et al., 2008; McKenney et al., 2007). However, climate change impacts will not be uniform for all species (Prasad et al., 2020), nor will they be uniform across a species' current distribution (Mathys et al., 2017; Rehfeldt et al., 2014a). For example, loss of suitable habitat at southern and low-elevation areas will not necessarily match gains at northern and high-elevation areas.

Forest ecosystems provide a wealth of ecological benefits and can serve as both economic and cultural resources for local communities. Protection of these resources through effective planning and management depends upon an informed understanding of how climate change may impact important tree species. In this study, we focused on five tree species that are important to the PNW and we assessed the potential impacts of four climate projections for the 2080s on the location of climatically suitable habitat for these species.

Five important species of the PNW

We selected five species based on their commercial, ecological, or cultural importance in the PNW and their expected vulnerability to projected changes in climate (Brown et al., 2018; Case & Lawler, 2016; Devine et al., 2012; Long et al., 2018): noble fir (*Abies procera*), coastal Douglas-fir (*Pseudotsuga menziesii* var. *menziesii*), blue oak (*Quercus douglasii*), Oregon white oak (*Quercus garryana*; hereafter, white oak), and California black oak (*Quercus kelloggii*; hereafter, black oak). Except for the geographic range of coastal Douglas-fir, which extends from southern California into British Columbia, Canada, the ranges of these species are primarily contained within the PNW. Coastal Douglas-fir is a major component of the timber industry in the PNW, supporting Oregon and Washington as the top softwood-lumber-producing states in the United States (Smith et al., 2009). Noble fir is an endemic, high-elevation species in the northern PNW and is managed for timber and bough production (Blatner et al., 2010; Franklin, 1990). Another endemic species to the south is blue oak, which occupies hot, dry foothill woodlands and is the most drought tolerant of California's deciduous oaks (McDonald, 1990). White oak woodlands and savannas are sparsely scattered across the PNW and extend slightly into British Columbia (Stein, 1990). Despite substantial habitat conversion from changes in land use and disturbance regimes, white oak woodlands continue to host high levels of species richness, including many at-risk species (Fuchs, 2001; Hahm et al., 2018; Pellatt et al., 2012). Black oak is an iconic species across California and southern Oregon and doubles as "both an ecological keystone and a cultural keystone" species (Long et al., 2016).

Multiple studies have highlighted the unique responses that these five species may have to climate change. For high-elevation species with limited upslope-migration options, such as noble fir, warmer temperatures are expected to negatively impact suitable habitat (Bell et al., 2014). The overall effect of climate change on coastal Douglas-fir's range size (i.e., area of its range) is projected to be small, with losses in suitable habitat expected at lower elevations and gains expected at higher elevations and northward into British Columbia (Gray & Hamann, 2013; Mathys et al., 2017; Rehfeldt et al., 2014a). However, Rehfeldt et al. (2014b) found that, while much of coastal Douglas-fir's habitat would remain climatically suitable by the 2060s, 18% of the projected future habitat is presently unoccupied by coastal Douglas-fir and an additional 24% is presently occupied by genetic stock that is projected to become maladapted.

Despite blue oak's drought tolerance, Brown et al. (2018) found end-of-century vulnerability for blue oak to be greatest to the south and in areas surrounding the Great Central Valley, where the frequency of drier years was projected to increase. Focusing on the northern portion of white oak's range and using observations from the 1930s onward, Pellatt et al. (2012) predicted climatically suitable habitat to increase by the end of this century, but that much of this future habitat would be spatially fragmented or occur in areas where white oak is currently in decline. Harsh sites, fragmentation, and other

threats to white oak's extant habitat have led to this species being identified as highly vulnerable to climate change (Case & Lawler, 2016; Devine et al., 2012). Impacts of climate change on black oak are less clear, although increased moisture stress is expected to negatively impact mature black oak, particularly toward the fringe of this species' range (Long et al., 2016; Lutz et al., 2010).

Utility of CAR models in bioclimatic SDMs

Species distribution models (hereafter, SDMs; Araújo & Peterson, 2012; Elith & Leathwick, 2009; Franklin, 2009) are often used to understand how climate change impacts may shift suitable habitat for tree species (e.g., Bell et al., 2014; Rehfeldt et al., 2014a). Bioclimatic SDMs use current climate data to estimate correlative relationships between a species' response (e.g., occurrence, abundance) and climate covariates representing the species' climatic habitat. The estimated species–climate relationships can then be applied to data from future climate scenarios to project how these scenarios would impact the geographic location of climatically suitable habitat.

Correctly identifying the relationship between a species and climate is an important step in building useful SDMs for climate change studies. The observed distribution of a species is not solely the result of climate, but rather a complex interaction of climate with other environmental and ecological factors (e.g., soils, disturbances, competition, dispersal). Often the direct, proximal variables representing influential factors are not available, and so appropriate surrogate variables are used (Austin, 2007). Information from such influential factors, which is not captured by surrogate variables in SDMs, may still be captured as spatially patterned error and expressed as spatial autocorrelation in model residuals (Cressie et al., 2009; Ver Hoef et al., 2018).

When data are associated with spatial areal units, we can incorporate spatial information into the modeling process with spatial conditional autoregressive (CAR) models (Besag, 1974). To encode spatial dependency, CAR models use neighbor relationships by specifying dependency conditional on observations at neighboring locations (Cressie, 1993; Ver Hoef et al., 2018). For example, spatial random effects for individual polygons (i.e., random intercepts) can be included in a Bayesian hierarchical generalized linear model (GLM), where the covariance matrix of the random effects uses a CAR model based on specified neighbor relationships (Ver Hoef et al., 2021). When SDMs are estimated with Markov chain Monte Carlo (MCMC) methods, spatial CAR models have the added benefit of allowing practitioners to map covariate and prediction uncertainty (Cressie et al., 2009). The ability to characterize prediction uncertainty is particularly appealing in climate change studies where it is common for projected impacts to be examined for multiple future climate scenarios.

The overall goal of our study was to develop species-specific SDMs for these five tree species, with the aim of providing realistic predictions of climatically suitable habitat and evaluating potential impacts of four climate projections for the 2080s. For each species, our specific objectives were to: (1) develop a spatial Bayesian hierarchical model to estimate spatial relationships (via a CAR model) between species and habitat based on species' presence–absence data and 30-year averages of current climate; (2) estimate the effect of climate covariates on the probability of species occurrence; (3) produce mapped predictions of climatically suitable habitat and mapped prediction uncertainty for the current and four future climate scenarios; and (4) evaluate impacts of climate change on the species' geographic range by assessing the estimated change in range size and examining the area expected to persist (remain suitable), expand (become suitable), or contract (become unsuitable) by the 2080s for the future climate scenarios. We outline an approach that provides characterizations of uncertainty when assessing climate change impacts, including estimates of covariate and prediction uncertainty.

METHODS

Study region

The study area covers the western states of California, Oregon, and Washington of the United States, hereafter referred to as the PNW. This region is composed of a broad range of climate conditions as latitudinal, orographic, and maritime influences interact to form a variety of temperature and precipitation regimes. The diverse environmental conditions of the PNW are expressed in a wide variety of vegetation types, ranging from temperate rain forests in northwest Washington to chaparral shrublands and deserts in southern California. Within this region, we focus on five tree species: noble fir, coastal Douglas-fir, blue oak, (Oregon) white oak, and (California) black oak.

Data and model forms

Field observations

The sample units in our study come from presence–absence observations on plots measured between 2001 and 2011 by

the Forest Inventory and Analysis (FIA) program. As part of a national monitoring program for forest vegetation, FIA field plots (hereafter, FIA plots) are randomly located within a tessellation of hexagonal spatial units, with each hexagon covering approximately 2400 ha. Across our study area, the median number of FIA plots per hexagon is one, with a maximum of five plots in national forests with spatial intensification. The FIA program only recorded species data on forested FIA plots and defined forested lands as areas with greater than 10% canopy cover or stocking on the acre. Although the ranges for three of our focal species are contained within forested lands, the ranges of blue oak and white oak extend into nonforested lands (i.e., areas not meeting the forested threshold). For clarity, we hereafter refer to FIA plots by the response type: observed FIA plots, which occur on forested lands where the species' occurrence was recorded, and unobserved FIA plots, which occur on naturally nonforested lands (e.g., rangeland) where species' occurrence was not recorded. In addition to observed FIA plots, which were included in all data sets, we included unobserved FIA plots in the data sets of blue oak and white oak. The conceptual relationship between FIA plots and hexagons is illustrated in Figure 1.

To protect landowner privacy and data integrity, some data collected on FIA plots are not made publicly available (e.g., true location; Burrill et al., 2021). We obtained permission to use the full data and were therefore able to associate FIA plots with their containing hexagon (for documentation and access information, see Burrill et al., 2021). Access to the full data also allowed us to associate FIA plots with their corresponding ecological section (ES; Cleland et al., 2007). These ES designations define large areas with similar physical and biological features, which are expected to respond similarly to disturbance (McNab et al., 2007). Although not a surrogate for populations, we expected that the average response of a species to climate would vary between ESs because of their unique ecological characteristics. A list of the ESs present in each species-specific data set is provided in Appendix S1: Section S1.

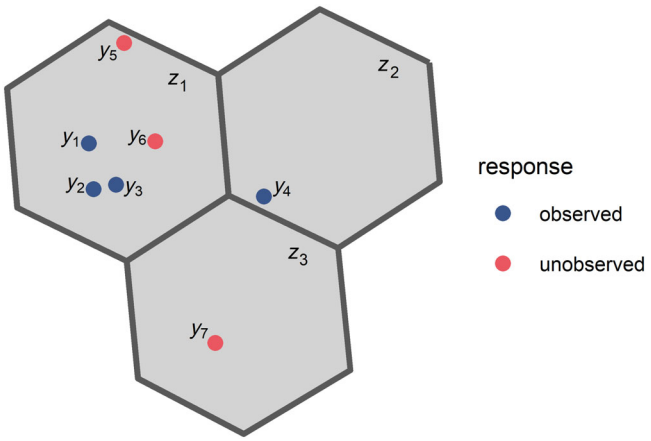

FIGURE 1 An example illustration of the relationship between Forest Inventory and Analysis (FIA) plots (sample units) and their containing hexagons (spatial units), where forested FIA plots are shown in blue (i.e., FIA plots where the species occurrence was recorded; an observed response) and nonforested FIA plots are shown in red (i.e., FIA plots where species occurrence was not recorded; an unobserved response). Only observed FIA plots were included in the data sets for noble fir, coastal Douglas-fir, and black oak, while both observed and unobserved FIA plots were included in data sets for blue oak and white oak. Subscripted labels (e.g., y_5, z_1) are used to demonstrate the structure of matrices in a spatial Bayesian hierarchical model.

Characteristics of the five species-specific data sets used in this study are presented in Table 1. For each species, FIA plots with absences or unobserved responses were only included if they occurred within 200 km of an FIA plot with a presence. Because FIA plot data do not distinguish between varieties for Douglas-fir, we differentiated the range of coastal Douglas-fir from the Rocky Mountain variety (var. *glauca*) based on genetic and migration findings in Gugger et al. (2010) and subsequently removed FIA plots within the Rocky Mountain variety's range. Finally, we removed any FIA plots occurring in isolated hexagons (i.e., those not sharing a common edge with another hexagon in the sample) from species-specific data sets. After the data sets were assembled, we classified hexagons as observed or unobserved: an observed hexagon contained at least one observed FIA plot and an unobserved hexagon contained only unobserved FIA plots. We discuss the rationale for removing isolated hexagons and classifying hexagons in the section Spatial Bayesian hierarchical model.

Present and future climate

Current climate data for FIA plots were obtained from PRISM (parameter-elevation relationships on independent slopes model) climate normals (30-year averages) of monthly and annual temperature and precipitation data for the period 1981–2010 at 800-m resolution (data set Norm81m; PRISM Climate Group, 2012). From these data, we calculated all bioclimatic variables (Hijmans, 2004; Nix, 1986) according to O'Donnell and Ignizio (2012). Of the two equations O'Donnell and Ignizio (2012) provide for temperature seasonality, we applied the standard deviation equation that aligns with Hijmans (2004). In addition to bioclimatic variables, we calculated variables for degree-days and a heat–moisture index (calculations provided in Table 2).

Future climate data were locally downscaled and generated with the ClimateNA version 5.21 software package

TABLE 1 Species abbreviations (abbrev) and summary statistics for the species-specific data sets. Summary statistics include observed prevalence (in percentage), number of observed (*o*) and unobserved (*u*) Forest Inventory and Analysis (FIA) plots and hexagons, and number of ecological sections (ESs).

			FIA plots		Hexagons		
Species	**Abbrev**	**Prevalence**	***o***	***u***	***o***	***u***	**ESs**
Noble fir	ABPR	3.5	15,126		10,161		20
Coastal Douglas-fir	PSMEM	53.8	16,144		11,790		22
Blue oak	QUDO	7.3	6719	6083	6124	6010	20
Oregon white oak	QUAG4	2.6	17,952	9579	12,957	9225	27
California black oak	QUKE	9.5	12,113		9290		25

TABLE 2 Description of climate covariates and their inclusion in fixed-effects model forms for noble fir (ABPR), coastal Douglas-fir (PSMEM), blue oak (QUDO), white oak (QUGA4), and black oak (QUKE).

		Fixed-effects model form				
Covariate	**Description**	**ABPR**	**PSMEM**	**QUDO**	**QUGA4**	**QUKE**
gdd5	Growing degree-days over 5°C[a]		X			X
hmi	Heat–moisture index[b,c]					
tmax-warmM	Max. temp. of warmest month[d]				**X**	**X**
tmin-coldM	Min. temp. of coldest month[d]			X		
tmean-wetQ	Mean temp. of wettest quarter[d]		**X**	**X**	**X**	**X**
tmean-warmQ	Mean temp. of warmest quarter[d]	**X**	**X**		**X**	
ppt-ann	Total annual precipitation[c,d]					
ppt-wetM	Precipitation of wettest month[d]					**X**
ppt-wetQ	Precipitation of wettest quarter[d]			**X**	**X**	
ppt-warmQ	Precipitation of warmest quarter[d]	**X**	**X**	**X**	**X**	

Note: Climate covariates that were included in a species' model (e.g., through a linear, quadratic, or interaction term) are indicated by an "X" in boldface if a term related to that covariate was significant in the final hierarchical model (zero excluded from equal-tailed 90% credible interval for the posterior mean); the fixed-effect intercepts were significant in final hierarchical models for all species.

[a]Sum of month-days for which mean temperature exceeded 5°C (i.e., frost-free days; in days).

[b]Index calculated as (tmean-ann + 10)/(ppt-ann/1000), where tmean-ann (annual mean temperature) was calculated as in O'Donnell and Ignizio (2012).

[c]Not included in the final model form for any of the species.

[d]See O'Donnell and Ignizio (2012) for calculation; units are temperature in degrees Celsius and precipitation in millimeters.

(available at https://sites.ualberta.ca/~ahamann/data/climatena.html), which is based on methodology described by Wang et al. (2016). We evaluated possible climate change impacts for four future climate scenarios for the 2080s (2071–2100 normal period), including two emission pathways and two climate models. We selected representative concentration pathways (RCPs; van Vuuren et al., 2011) that represent an intermediate emissions pathway in which radiative forcing stabilizes around the year 2100 (RCP 4.5, stabilizing at approximately 4.5 W/m^2 by 2100) and a high emissions pathway in which radiative forcing continues to rise after 2100 for some time (RCP 8.5, exceeds 8.5 W/m^2 by 2100).

To interpret each emission pathway, we selected two climate models (atmosphere–ocean general circulation models; AOGCMs). We compared the AOGCMs available through ClimateNA and chose the AOGCMs that represented a median (CCSM4; NCAR Community Climate System Model, version 4.0; Gent et al., 2011) and a worst-case (HadGEM2-ES; Met Office Hadley Centre Global Environmental Model, version 2, Earth System; Jones et al., 2011) climate projection. For this comparison, we examined projected changes between the 1970s (1961–1990 normal period) and the 2050s (2041–2070 normal period) in state-level (i.e., California, Oregon, and Washington) mean annual temperature and mean annual precipitation under the intermediate emission pathway (i.e., RCP 4.5; data accessed from the ClimateNA website). Temperature was projected to increase by the 2050s under all AOGCMs but changes in

precipitation were more variable. When AOGCMs were sorted by the magnitude of projected temperature change, the CCSM4 model had a median projection while the HadGEM2-ES had one of the warmest projections (worst case). Although both models generally projected drier conditions by the 2050s, neither model had the most extreme projected increase nor decrease in precipitation when compared with the other AOGCMs.

Identifying model forms

After identifying climate covariates that were physiologically meaningful to each species, model forms were determined by fitting nonspatial, logistic generalized linear mixed models (GLMMs) on all covariates with a fixed intercept and a random intercept for ES. All 10 climate covariates listed in Table 2 were initially considered for blue oak and black oak, while all but ppt-wetM (precipitation of wettest month) were considered for the other three species. Covariates were standardized (centered and divided by their standard deviation) before model fitting, and covariate standardizations were recorded and applied to future climate data sets for prediction. Both linear and quadratic terms were considered for bioclimatic variables to allow for unimodal response curves, except for gdd5 (growing degree-days over 5°C) for which we only considered linear terms. To allow for the effect of precipitation to vary with mean temperature, we considered interaction terms for precipitation and mean temperature variables within a similar period, for example, wettest quarter or month (e.g., tmean-warmQ and ppt-warmQ, tmean-wetQ and ppt-wetQ, tmean-wetQ and ppt-wetM). Covariates included in final model forms were identified by successively removing covariates when all parameters associated with a specific covariate were not significant (0.1 level) and removal resulted in an improvement in Akaike information criterion (Akaike, 1973). The climate covariates included in the final model forms are described in Table 2.

Spatial Bayesian hierarchical model

We used spatial Bayesian hierarchical models to examine the effect of climate covariates and predict climatically suitable habitat for each species. We denote the vector of species' response at the FIA plots $\boldsymbol{y}$, for which the Bernoulli response (i.e., presence or absence) was observed or, if the species was blue oak or white oak, possibly unobserved (i.e., unknown response). We related the response at an FIA plot to the climate covariate data, ES membership, and hexagon membership for that FIA plot through the following hierarchical model:

$$\boldsymbol{y} \sim [\boldsymbol{y}|\boldsymbol{\beta},\boldsymbol{\nu},\boldsymbol{z},\mathbf{X},\mathbf{Q},\mathbf{U}] \equiv \text{Bernoulli}(\boldsymbol{\mu}) \text{ with } \boldsymbol{\mu} \equiv g^{-1}(\boldsymbol{\eta}), \tag{1}$$

$$\boldsymbol{\eta} \equiv \mathbf{X}\boldsymbol{\beta} + \mathbf{Q}\boldsymbol{\nu} + \mathbf{U}\boldsymbol{z}, \tag{2}$$

$$\boldsymbol{\nu} \sim [\boldsymbol{\nu}|\sigma_\nu] \equiv \text{MVN}\left(\mathbf{0}, \sigma_\nu^2\mathbf{I}\right), \tag{3}$$

$$\boldsymbol{z} \sim [\boldsymbol{z}|\boldsymbol{\theta}] = [\boldsymbol{z}|\rho,\sigma_z] \equiv \text{MVN}(\mathbf{0}, \boldsymbol{\Sigma}_{\boldsymbol{\theta}}), \tag{4}$$

$$\boldsymbol{\Sigma}_{\boldsymbol{\theta}} \equiv \sigma_z^2(\text{diag}(\mathbf{W}\mathbf{1}) - \rho\mathbf{W})^{-1} \equiv \sigma_z^2\mathbf{R}_\rho^{-1}, \tag{5}$$

where the bracket notation [...] denotes a probability distribution of the variable on the left of the symbol | conditional on the variables or parameters to the right of that symbol (Gelfand & Smith, 1990). Here, the mean response vector $\boldsymbol{\mu}$ is related to the linear predictor $\boldsymbol{\eta}$ by the inverse-logit function g^{-1}. The vector $\boldsymbol{\eta}$ is related to the design matrix $\mathbf{X}$ containing the climate covariate data for the FIA plots with fixed-effects regression coefficients $\boldsymbol{\beta}$, the design matrix $\mathbf{Q}$ containing 0s and 1s for ES random effects $\boldsymbol{\nu}$, and the design matrix $\mathbf{U}$ containing 0s and 1s that match FIA plots with their hexagon's spatial random effect (elements of $\boldsymbol{z}$).

We assumed that both $\boldsymbol{\nu}$ and $\boldsymbol{z}$ follow multivariate normal distributions and that the distribution of the spatial random effects ($\boldsymbol{z}$) depends on the covariance matrix $\boldsymbol{\Sigma}_{\boldsymbol{\theta}}$ through the parameter vector $\boldsymbol{\theta} = (\rho,\sigma_z)'$. Following Ver Hoef et al. (2018), we modeled this dependence with a row-standardized CAR model. In Equation (5), the function diag creates a diagonal matrix; $\mathbf{W}$ is a matrix encoding neighbor relationships; $\mathbf{1}$ is a vector of ones; and $\mathbf{R}_\rho$ denotes the single matrix for the row-standardized CAR model that is dependent on the parameter ρ. We used a first-order neighbor structure for $\mathbf{W}$ and encoded neighboring hexagons by 1 and non-neighbors by 0. We defined neighbors as any two hexagons sharing a common edge, which translated to a maximum of six neighbors for an individual hexagon. Because a row of zeros in $\mathbf{W}$ would be problematic, we removed isolated hexagons (and all FIA plots within these hexagons) from species-specific data sets before model fitting. Although other options for handling isolated spatial units exist (Ver Hoef et al., 2018), we had relatively few isolated hexagons (0.4%–2.0% depending on the data set) and the removal of associated FIA plots did not greatly impact our overall sample size.

Row-standardized CAR models tend to estimate a greater marginal variance for spatial units (hexagons) with fewer neighbors (Ver Hoef et al., 2018). Assuming greater uncertainty toward the perimeter of sample locations is reasonable when the entire geographic range of a species is represented in the sample data. However, such

CAR models can still be applicable if the species' response is partly unobserved (i.e., blue oak and white oak) or if the species' range extends beyond the study area's extent (i.e., coastal Douglas-fir). For blue oak and white oak, greater marginal variances in observed hexagons toward the interior of the species range can be stabilized by including covariate data from FIA plots in unobserved hexagons. Because the range of coastal Douglas-fir is truncated in our data set at the Canadian border, we know to expect greater marginal variances in (observed) hexagons along the northern extent of our study area.

For computational savings during model fitting, we write $\boldsymbol{z} = (\boldsymbol{z}_o', \boldsymbol{z}_u')'$ where $\boldsymbol{z}_o$ and $\boldsymbol{z}_u$ are vectors of spatial random effects associated with observed hexagons and unobserved hexagons, respectively (Ver Hoef et al., 2021). If the response on all FIA plots was observed (i.e., noble fir, coastal Douglas-fir, and black oak), then $\boldsymbol{z}_u$ is a zero-length vector and $\boldsymbol{z} = \boldsymbol{z}_o$.

The response vector $\boldsymbol{y}$ can be partitioned as $\boldsymbol{y} = (\boldsymbol{y}_o', \boldsymbol{y}_u')'$ into the responses on observed ($\boldsymbol{y}_o$) and unobserved ($\boldsymbol{y}_u$) FIA plots. As illustrated in Figure 1, unobserved FIA plots for white oak and blue oak may occur in observed or unobserved hexagons. We can similarly structure $\mathbf{X}$, $\mathbf{Q}$, and $\mathbf{U}$ to be partitionable by the observed or unobserved FIA plots. For $\mathbf{X}$ and $\mathbf{Q}$, we have

$$\mathbf{X} = \begin{bmatrix} \mathbf{X}_o \\ \mathbf{X}_u \end{bmatrix} \text{ and} \tag{6}$$

$$\mathbf{Q} = \begin{bmatrix} \mathbf{Q}_o \\ \mathbf{Q}_u \end{bmatrix}, \tag{7}$$

where $\mathbf{X}_o$ and $\mathbf{X}_u$ are matrices with the same number of columns as $\mathbf{X}$ and number of rows corresponding to the length of $\boldsymbol{y}_o$ and $\boldsymbol{y}_u$, respectively; that is, $\mathbf{X}_o$ and $\mathbf{X}_u$ are the design matrices with climate covariate data corresponding to the FIA plots with observed and unobserved responses, respectively. The same notation holds for $\mathbf{Q}$ where $\mathbf{Q}_o$ and $\mathbf{Q}_u$ are design matrices encoding ES membership for FIA plots with observed and unobserved responses, respectively. Because $\mathbf{U}$ matches FIA plots to hexagons, we can further partition $\mathbf{U}$ for blue oak and white oak by the observed or unobserved hexagons,

$$\mathbf{U} = \begin{bmatrix} \mathbf{U}_o \\ \mathbf{U}_u \end{bmatrix} = \begin{bmatrix} \mathbf{U}_{o,o} & \mathbf{U}_{o,u} \\ \mathbf{U}_{u,o} & \mathbf{U}_{u,u} \end{bmatrix}, \tag{8}$$

where a matrix's two-letter subscript indicates the type of response on the FIA plot and the type of hexagon being matched through that matrix; for example, $\mathbf{U}_{u,o}$ matches FIA plots with an unobserved response ($\boldsymbol{y}_u$) with the random effects for observed hexagons ($\boldsymbol{z}_o$). For noble fir, coastal Douglas-fir, and black oak, we have $\mathbf{X} = \mathbf{X}_o$, $\mathbf{Q} = \mathbf{Q}_o$, and $\mathbf{U} = \mathbf{U}_{o,o}$. Because observed FIA plots cannot occur within unobserved hexagons (by definition), $\mathbf{U}_{o,u}$ is always a matrix of zeros. To illustrate this concept, suppose Figure 1 showed all plots within the blue oak data set, then the components of Equation (8) are written as

$$\mathbf{U}_{o,o} = \begin{bmatrix} 1 & 0 \\ 1 & 0 \\ 1 & 0 \\ 0 & 1 \end{bmatrix}, \quad \mathbf{U}_{o,u} = \begin{bmatrix} 0 \\ 0 \\ 0 \\ 0 \end{bmatrix}, \quad \mathbf{U}_{u,o} = \begin{bmatrix} 1 & 0 \\ 1 & 0 \\ 0 & 0 \end{bmatrix}, \text{ and}$$

$$\mathbf{U}_{u,u} = \begin{bmatrix} 0 \\ 0 \\ 1 \end{bmatrix},$$

where the elements of $\boldsymbol{y}$ and $\boldsymbol{z}$ are ordered according to the subscripts in Figure 1.

Assuming conditional independence between the elements of $\boldsymbol{y}$, we can write Equation (1) as

$$\begin{aligned} &[\boldsymbol{y}|\boldsymbol{\beta}, \boldsymbol{\nu}, \boldsymbol{z}, \mathbf{X}, \mathbf{Q}, \mathbf{U}] \\ &= [\boldsymbol{y}_o|\boldsymbol{\beta}, \boldsymbol{\nu}, \boldsymbol{z}_o, \boldsymbol{z}_u, \mathbf{X}_o, \mathbf{Q}_o, \mathbf{U}_o][\boldsymbol{y}_u|\boldsymbol{\beta}, \boldsymbol{\nu}, \boldsymbol{z}_o, \boldsymbol{z}_u, \mathbf{X}_u, \mathbf{Q}_u, \mathbf{U}_u]. \end{aligned} \tag{9}$$

Then, the joint posterior distribution based on the observed response data for all parameters is

$$\begin{aligned} &[\psi|\mathbf{X}_o, \mathbf{Q}_o, \mathbf{U}_o, \boldsymbol{y}_o] = [\boldsymbol{\beta}, \rho, \sigma_z, \sigma_v, \boldsymbol{\nu}, \boldsymbol{z}_o, \boldsymbol{z}_u|\mathbf{X}_o, \mathbf{Q}_o, \mathbf{U}_o, \boldsymbol{y}_o] \\ &\propto [\boldsymbol{y}_o|\boldsymbol{\beta}, \boldsymbol{\nu}, \boldsymbol{z}_o, \boldsymbol{z}_u, \mathbf{X}_o, \mathbf{Q}_o, \mathbf{U}_o][\boldsymbol{z}_o, \boldsymbol{z}_u|\rho, \sigma_z][\boldsymbol{\nu}|\sigma_v][\boldsymbol{\beta}][\sigma_z][\sigma_v][\rho], \end{aligned} \tag{10}$$

where $\psi = (\boldsymbol{\beta}', \rho, \sigma_z, \sigma_v, \boldsymbol{\nu}', \boldsymbol{z}_o', \boldsymbol{z}_u')'$ is a vector containing model parameters and we specify flat infinite priors for the components of $\boldsymbol{\beta}$ and flat priors for $\rho \in (0,1)$, $\sigma_z \in (0, \infty)$, and $\sigma_v \in (0, \infty)$. Based on (9) and (10), the posterior predictive distributions of the observed and unobserved FIA plots are:

$$\begin{aligned} [\tilde{\boldsymbol{y}}_o, \tilde{\mathbf{X}}_o, \mathbf{Q}_o, \mathbf{U}_o|\boldsymbol{y}_o] = \int_\psi &[\tilde{\boldsymbol{y}}_o, \boldsymbol{\beta}, \boldsymbol{\nu}, \boldsymbol{z}_o, \boldsymbol{z}_u, \tilde{\mathbf{X}}_o, \mathbf{Q}_o|\mathbf{U}_o] \\ &[\psi|\mathbf{X}_o, \mathbf{Q}_o, \mathbf{U}_o, \boldsymbol{y}_o] d\psi \text{ and} \end{aligned} \tag{11}$$

$$\begin{aligned} [\tilde{\boldsymbol{y}}_u, \tilde{\mathbf{X}}_u, \mathbf{Q}_u, \mathbf{U}_u|\boldsymbol{y}_o] = \int_\psi &[\tilde{\boldsymbol{y}}_u, \boldsymbol{\beta}, \boldsymbol{\nu}, \boldsymbol{z}_o, \boldsymbol{z}_u, \tilde{\mathbf{X}}_u, \mathbf{Q}_u|\mathbf{U}_u] \\ &[\psi|\mathbf{X}_o, \mathbf{Q}_o, \mathbf{U}_o, \boldsymbol{y}_o] d\psi, \end{aligned} \tag{12}$$

respectively, where the tilde denotes a new set of data; that is, $\tilde{\boldsymbol{y}}_o$ and $\tilde{\boldsymbol{y}}_u$ can be interpreted as new species response (presence or absence) at the observed and

unobserved FIA plots for the new climate covariate data contained in $\tilde{\mathbf{X}}_o$ and $\tilde{\mathbf{X}}_u$, respectively. Note that the integrand on the right-hand side of Equations (11) and (12) is the product of the data model and the posterior distribution.

Model fitting

Species-specific models were fit with MCMC methods using a Metropolis–Hastings sampler (Hastings, 1970; Metropolis et al., 1953) in R (R Core Team, 2020); for an overview of MCMC methods, see Gilks et al. (1996). Our MCMC scheme implemented the time-saving innovations outlined in Ver Hoef et al. (2021), including splitting $\boldsymbol{z}_o$ and $\boldsymbol{z}_u$, use of sparse matrices in block sampling, and use of lookup tables. Proposal distributions were centered on a parameter's sample from the previous iteration and tuned so that acceptance rates stayed between 0.2 and 0.5. We used Gaussian proposals for the components of $\boldsymbol{\beta}$, $\boldsymbol{z}_o$, $\boldsymbol{z}_u$, and $\boldsymbol{\nu}$, uniform proposals for σ_z and σ_ν, and a discrete uniform proposal for ρ. Block proposals were used for $\boldsymbol{z}_o$, $\boldsymbol{z}_u$, and $\boldsymbol{\nu}$. To ensure identifiability from the fixed-effect intercept (β_0), an additional constraint was placed on $\boldsymbol{\nu}$ to be centered at zero; this was accomplished by centering the components of $\boldsymbol{\nu}$ following proposal draws. To speed likelihood computations for the determinant and inverse of $\boldsymbol{\Sigma}_{\boldsymbol{\theta}}$, we used a lookup table for $\mathbf{R}_\rho$ based on 101 values of ρ between 0 and 1 evenly spaced from −8 and 8 along the logit scale. The discrete uniform proposal for ρ was therefore based on these 101 values. No boundary issues were observed in our study for parameters with constraints (i.e., ρ, σ_z, and σ_ν).

To further increase the speed of model convergence, spatial random effects were sampled at a higher rate (50:1) than other model parameters. For each complete iteration across all model parameters, we kept the last sample of $\boldsymbol{z}_o$ and $\boldsymbol{z}_u$. For clarity, we hereafter use the term iteration to refer to a single complete sample across all model parameters. Following a burn-in of 200,000 iterations, we ran the sampler for 1,000,000 iterations and kept every 500th sample; this resulted in 2000 samples from the joint posterior distribution.

To assess if models converged to a stationary posterior distribution, we examined trace plots and summary statistics for the parameters. Because of the large number of random effects, examining individual trace plots was not practical for $\boldsymbol{z}_o$, $\boldsymbol{z}_u$, and $\boldsymbol{\nu}$. Instead, summary statistics (mean and interquartile range) and a subset of these parameters' trace plots were examined. For the trace plots, we chose a subset that was representative of both extremes and common conditions within the data set (e.g., varying numbers of FIA plots and observed presences, and both observed and unobserved hexagons). Further details on the MCMC sampling procedure are included in Appendix S1: Section S2.

Model predictions

With the 2000 MCMC samples from the joint posterior distribution, we generate predictions for each of the five climate data sets (current and four future climate scenarios) by updating the climate covariate data contained $\mathbf{X}$. For a given climate scenario, we write the vector of predicted probabilities for the kth MCMC sample as $\boldsymbol{\mu}^k = g^{-1}(\boldsymbol{\eta}^k)$ where, recalling that g^{-1} is the element-wise inverse logit, the vector $\boldsymbol{\eta}^k$ is calculated based on Equation (2) as

$$\boldsymbol{\eta}^k = \mathbf{X}\boldsymbol{\beta}^k + \mathbf{Q}\boldsymbol{\nu}^k + \mathbf{U}\boldsymbol{z}^k, \tag{13}$$

where the superscript k indicates the vectors $\boldsymbol{\beta}^k$, $\boldsymbol{\nu}^k$, and $\boldsymbol{z}^k$ come from the kth MCMC sample and $\mathbf{X}$ contains the climate covariate data for the specified climate scenario. We map $\boldsymbol{\mu}^k$ by associating predictions with their FIA plot locations. Repeating this process for all 2000 MCMC samples yields 2000 prediction maps for that specific climate scenario.

We interpret the $\boldsymbol{\mu}^k$ predictions as the probability of presence with respect to climatically suitable habitat, hereafter the probability of climatically suitable habitat. Predictions depend on the model's estimation of the current species–climate relationship, effect of ES, and spatial effects. We assumed that spatially patterned error at the hexagon level from unaccounted-for influential factors (e.g., competition, soils) will not change substantially by the 2080s. Although climate change may impact factors expressed through the model's spatial component, we consider the model's estimation of the current spatial effects to be an informed "better guess" of future spatial effects. Therefore, we used the MCMC samples of the spatial random effects for prediction in Equation (13). Rather than projecting the location of a species' presence in the 2080s, we believe the projections represent the probability of climatically suitable habitat, with some adjustment for present-day spatial and ES effects.

Additionally, because observations of species' presence in the FIA data were limited to forested lands, predictions should be interpreted within this context. For example, the hottest and driest part of blue oak's current range is in areas that could be classified as blue oak savannah, where the canopy cover or stocking on the acre may be less than 10% (i.e., nonforested lands). While we include covariate data from nonforest areas for blue oak and white oak to obtain more realistic estimates of

uncertainty along the forest/nonforest boundary, no species response data are collected at these locations. Therefore, while a location may be predicted as unsuitable for forest-land blue oak, that same location may not be unsuitable for blue oak savannah.

For each species and climate scenario, we mapped the mean-predicted probability for each FIA plot across the MCMC samples and refer to this as the mean-prediction map. That is, for the *i*th FIA plot, we found the mean of the predicted probabilities across all 2000 prediction maps,

$$\bar{\mu}_i = \sum_{k}^{2000} \mu_i^k / 2000, \tag{14}$$

where μ_i^k is the predicted probability at the *i*th FIA plot based on the *k*th MCMC sample. Because the mean-prediction map is an average of the 2000 prediction maps, it is possible that patterns expressed in the mean-prediction map will not be expressed in any individual prediction map. Therefore, the mean-prediction map should be interpreted in parallel with a corresponding map of prediction uncertainty. We mapped the standard error (SE) of prediction for each FIA plot and refer to this as the uncertainty map. That is, for the *i*th FIA plot, we found the SE of prediction across all 2000 prediction maps,

$$\widehat{\mathrm{SE}}(\bar{\mu}_i) = \sqrt[2]{\sum_{k}^{2000} (\mu_i^k - \bar{\mu}_i)^2 / (2000 - 1)}. \tag{15}$$

Model assessment

Following model convergence, we evaluated the univariate effective sample size (ESS; Kass et al., 1998; Robert & Casella, 2004) for each parameter. Because MCMC samples are autocorrelated, the univariate ESS for a parameter is the effective number of independent samples that would be produced with the same SE. A conservative estimate of the overall ESS is the minimum univariate ESS of all parameters (i.e., the univariate ESS of the parameter that mixed slowest). The minimum univariate ESS can then be used to determine if the sampler was stopped too soon and more MCMC samples are required. We chose to compare the minimum univariate ESS to a threshold of 30 effective independent samples for the slowest mixing parameter.

In addition to MCMC diagnostics (e.g., ESS), model diagnostics were examined to assess model performance and check underlying model assumptions (Conn et al., 2018). We used area under the receiver operating characteristic curve (AUC; Hanley & McNeil, 1982) to assess predictive performance and used a model check based on Moran's *I* (Moran, 1950) to determine if the CAR models adequately accounted for spatial autocorrelation. Because occupancy was unknown at unobserved FIA plots, only observed FIA plots were used in AUC and Moran's *I* model check calculations. The AUC statistic is threshold independent and measures the model's ability to discriminate between occupied and unoccupied sites. An AUC of 1 indicates perfect prediction, while values near 0.5 indicate that the model is classifying presence or absence at random. We calculated AUC for each MCMC sample with the R package pROC (version 1.17.0.1; Robin et al., 2011). For the model check, we used Moran's *I* to quantify unaccounted-for spatial autocorrelation in model "residuals" at eight discrete distance classes. Following Wright et al. (2019), we defined the "residual" at an FIA plot as the observed response minus the predicted probability. Because the calculation of Moran's *I* was computationally intensive, we only considered 100 MCMC samples (every 20th sample of the 2000 MCMC samples) in our calculations. We grouped pairs of FIA plots by the planar distance between pairs into one of eight classes: 0–5 km, 5–10 km, 10–15 km, 15–25 km, 25–50 km, 50–100 km, 100–200 km, or >200 km. For each distance class, correlation in model "residuals" was then measured by calculating Moran's *I* for FIA plot pairs within that distance class. If the CAR model (i.e., spatial component of the model) adequately accounted for spatial autocorrelation, then we expect the Moran's *I* model check to be near zero for all distance classes.

Species response curves and optimal conditions

To identify climate covariates that were significant in the model, we examined the posterior distribution of the climate covariate effects (i.e., components of $\boldsymbol{\beta}$); covariate effects were significant if an equal-tailed 90% credible interval for the posterior mean did not include zero. To assess whether the estimated species–climate relationships agreed with theory, we examined the species response curves (i.e., conditional effect of climate covariates on the species' response) fit by the MCMC samples to both univariate and bivariate climate gradients. Bivariate relationships were considered for climate covariates associated with an interaction term and univariate relationships were considered for all other climate covariates. To fit response curves for each MCMC sample, we held the random effects and any uninvolved covariates at zero (i.e., the prior mean of the random effects and the mean of the standardized covariates) and generated gridded climate data. Climate data for

univariate relationships were generated as 100 values, evenly spaced between the climatic extremes of the five climate data sets; climate data were similarly generated for bivariate relationships on a 100×100 grid. Following this process, 2000 response curves were fit for each univariate or bivariate relationship.

We then estimated optimal climate conditions for the species based on the fitted species response curves and compared these estimates to observed climate conditions for these species. To estimate optimal conditions for each MCMC sample, we analytically solved for the inflection point of each fitted response curve and excluded any inflection points that were not maxima. Because climate conditions for an analytical maximum can be unrealistic (e.g., ppt-warmQ < 0 mm), we further excluded maxima outside of the climatic extremes of the current or future climate data. With the resulting set of optima, we estimated the mode of optimal conditions as the value that maximized a kernel density estimate of the distribution of optimal conditions; kernel density estimation was performed with the R package ks (version 1.11.7; Duong, 2020) for a grid restricted to climate conditions represented by the optima. For univariate relationships, we additionally reported the 5th and 95th percentile of the estimated optimal climate conditions. We did not estimate optimal conditions for gdd5 because only a linear term was considered for this covariate.

Climate change impacts on range

We examined the change in the species' range (geographic distribution) and range size (area) to evaluate the impact of future climate scenarios on climatically suitable habitat. To estimate a species' range for each scenario and MCMC sample, we first simulated species occurrence (presence or absence) at observed and unobserved FIA plots from the posterior predictive distributions presented in Equations (11) and (12). Specifically, for a given scenario and the kth MCMC sample, the vector of posterior predictive simulations (PPS) at the FIA plots is

$$\tilde{\boldsymbol{y}}^k \sim \text{Bernoulli}\left(\tilde{\boldsymbol{\mu}}^k\right) \text{ with } \tilde{\boldsymbol{\mu}}^k \equiv g^{-1}\left(\tilde{\boldsymbol{\eta}}^k\right), \tag{16}$$

where the vector $\tilde{\boldsymbol{y}}^k = \left(\tilde{\boldsymbol{y}}_o^{k\prime}, \tilde{\boldsymbol{y}}_u^{k\prime}\right)'$ with $\tilde{\boldsymbol{y}}_o^k$ and $\tilde{\boldsymbol{y}}_u^k$ simulated from Equations (11) and (12), respectively, with model parameters from the kth MCMC sample; $\tilde{\boldsymbol{\eta}}^k$ is calculated as in Equation (13) with $\tilde{\mathbf{X}}_o$ and $\tilde{\mathbf{X}}_u$ updated to contain the climate covariate data corresponding to the specific climate scenario. We then estimated a species' range based on the PPS for that scenario and MCMC sample. Because estimates of climate change impacts might vary based on the range estimation method used, we explored two methods of range estimation: bivariate kernel density estimation (BKDE) and Voronoi polygons. However, we found both methods generally produced similar results for climate change impacts on range size. For brevity, we therefore focused on the BKDE method and present the Voronoi polygon method in Appendix S1: Section S3.

To estimate range with the BKDE method, we first aggregated PPS to the hexagon level and associated simulations with the hexagon's centroid to minimize the impact of clustered FIA plots on range estimates. For aggregation, we assigned a hexagon-level presence if any of the FIA plots within that hexagon had a simulated presence. Kernel density estimation and bandwidth selection were performed with the R package ks (Duong, 2020). We used a bivariate Gaussian kernel and a two-stage plug-in selector with an unconstrained pilot bandwidth for a full bandwidth matrix (Chacón & Duong, 2010). The bandwidth matrix controls the amount and direction of smoothing and its choice can substantially impact density estimation (Gitzen et al., 2006). Our choice of plug-in selector is better suited to handling complex multimodal densities (unconstrained) with probability mass concentrations not necessarily parallel to axes (full bandwidth) than constrained pilot bandwidth or diagonal bandwidth options (Chacón & Duong, 2010). For each species, we selected one bandwidth matrix based on observed presences (aggregated like PPS to the hexagon level), which was then applied in kernel estimation for all scenarios and MCMC samples. Fixing the bandwidth matrix in this manner ensures that uncertainty in range estimates is solely due to variation in MCMC samples, rather than also reflecting variation in bandwidth matrix selection.

Following kernel estimation, we extracted the polygons corresponding to the upper 95% contour of the bivariate kernel density estimate. We restricted these polygons to the area contained by the union of hexagons within that species' data set and further excluded any potential overlap with the Pacific Ocean, Puget Sound, or land area outside the PNW region. We then estimated the range as the resulting polygons and estimated range size as the summed area of these polygons. This process resulted in a posterior distribution of range size estimates for each scenario.

To assess the overall impacts of a future scenario on range size, we examined the posterior distribution of the change in range size and relative change in range size (i.e., change in range size relative to the current estimate of range size). To obtain samples from these posterior distributions, for each MCMC sample we calculated change in range size as the difference between the future and current range size estimates and relative change as this

difference divided by the current estimate. We considered a projected increase or decrease in range size to be significant if the equal-tailed 90% credible interval for the posterior mean excluded zero.

Although overall change in range size (as a surrogate for the area of climatically suitable habitat) is informative, it is not likely to capture all the features of climate impacts on suitable habitat. For example, it is possible to project a significant decrease in range size, but the amount of area that will become climatically unsuitable and the locations where a shift in suitability is expected could vary substantially among the 2000 prediction maps. Similarly, it is possible for a species to maintain the same range size under a future scenario and yet have no overlap with the current range. Therefore, we examined the area of overlap and change in range estimates between current and future scenarios. For each MCMC sample, we calculated the area projected to remain climatically suitable (range persistence), become climatically suitable (range expansion), or become climatically unsuitable (range contraction) by the 2080s; the relationship between range persistence, expansion, and contraction is illustrated in Figure 2. We then visualized the relationship between the expansion and contraction and estimated posterior means and equal-tailed 90% credible intervals for the area of range expansion, contraction, and persistence. We also estimated posterior means and equal-tailed 90% credible intervals for these area estimates relative to the current range size estimate (e.g., the area of range contraction by 2080s relative to the species' current range size).

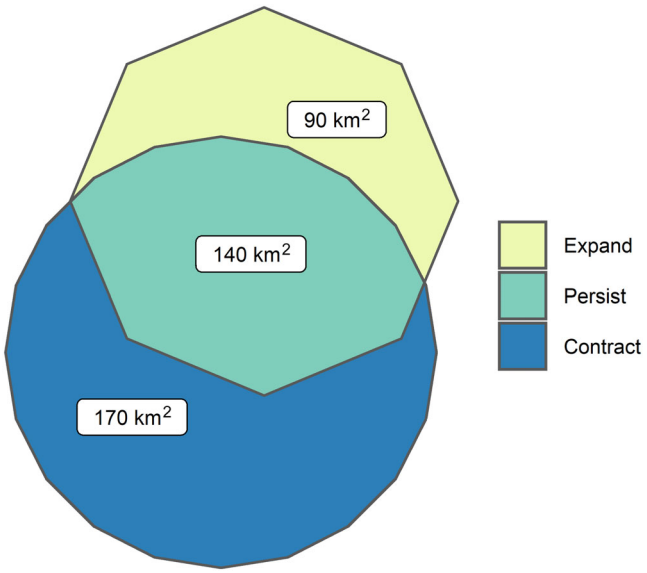

FIGURE 2 Conceptual relationship between the area of range contraction, persistence, and expansion. In this example, the current range size was 310 km² (i.e., sum of range persistence and contraction area) and the future range size was 230 km² (sum of range persistence and expansion area).

RESULTS

In this section, we first report on general model assessment, parameter significance, and estimated species–climate relationships. We then present mapped mean-predictions and uncertainty in predicted climatically suitable habitat for the current and four future climate scenarios. Finally, we turn our attention to range size estimates and the projected impact of climate scenarios on climatically suitable habitat for the 2080s. To be concise, we use coastal Douglas-fir as an illustrative example throughout and provide figures for the four other species in the Appendices.

Model assessment

Summaries of MCMC and model diagnostics are presented in Table 3. All models had an ESS of at least 31 (univariate ESS) for the slowest converging parameter and larger univariate ESS for most other parameters. Additionally, all models had strong predictive performance in differentiating between occupied and unoccupied sites with a minimum AUC of at least 0.95 across MCMC samples. The Moran's *I* model check showed that the models fit well across all eight distance classes we considered (i.e., model check values near zero, indicating minimal unaccounted-for spatial autocorrelation in model residuals). The largest deviation of the model check from zero was −0.04 for an MCMC sample from the noble fir model at the 0–5 km distance class, for which the mean model check value was −0.01.

In all models, all climate covariates had at least one corresponding regression coefficient that was significant, except for gdd5 and tmin-coldM (Table 2). For coastal Douglas-fir, the fixed-effects model form is

$$\begin{aligned} &-\mathbf{3.99} + 0.05(\text{gdd5}_{\text{std}}) + \mathbf{0.97}(\text{tmean-wetQ}_{\text{std}}) \\ &-\mathbf{0.66}(\text{tmean-wetQ}_{\text{std}})^2 + \mathbf{1.19}(\text{tmean-warmQ}_{\text{std}}) \\ &-\mathbf{0.44}(\text{tmean-warmQ}_{\text{std}})^2 + \mathbf{0.57}(\text{ppt-warmQ}_{\text{std}}) \\ &-\mathbf{0.18}(\text{ppt-warmQ}_{\text{std}})^2 \\ &+\mathbf{0.21}(\text{tmean-warmQ}_{\text{std}} \times \text{ppt-warmQ}_{\text{std}}), \end{aligned} \tag{17}$$

where coefficients in Equation (17) have been written as their posterior means (rounded to the nearest hundredth), the subscript std indicates that covariates are standardized, and coefficients in boldface were significant; similar equations for the other four species are provided in Appendix S1: Section S4.

TABLE 3 Summary statistics of Markov chain Monte Carlo (MCMC) and model diagnostics by species (model), including univariate effective sample size (ESS) summaries, minimum area under the receiver operating characteristic curve (AUC) across MCMC samples, and Moran's *I* model check summaries.

	Univariate ESS							
Model	**β**	ρ	σ_z	σ_v	z	v	**AUC**	**Model check**
ABPR	36 (183)	44	36	41	31 (114)	36 (41)	0.96	0.01 (12.8 km)
PSMEM	36 (119)	52	38	98	31 (158)	33 (40)	0.95	0.02 (3.5 km)
QUDO	64 (126)	38	31	175	31 (91)	51 (237)	0.98	0.01 (3.7 km)
QUGA4	70 (115)	45	31	147	31 (89)	49 (136)	0.98	0.00 (3.5 km)
QUKE	83 (205)	47	35	133	34 (273)	67 (115)	0.96	0.01 (3.5 km)

Note: Species include noble fir (ABPR), coastal Douglas-fir (PSMEM), blue oak, (QUDO), white oak (QUGA4), and black oak (QUKE). For the components of $\boldsymbol{\beta}$, $\boldsymbol{z}$, and $\boldsymbol{v}$, the univariate ESS of the slowest converging parameter is reported with the median univariate ESS in parentheses. For each model, the distance class with the greatest absolute mean value of the Moran's *I* model check (i.e., mean of 100 MCMC samples) is reported; the mean distance (in kilometers) between Forest Inventory and Analysis (FIA) plot pairs in that distance class is reported in parentheses.

The posterior mean of ρ was greater than 0.97 in all models. The posterior mean of σ_z was smallest in the blue oak model (1.8) and largest in the white oak model (2.6). The posterior mean of σ_v was greater in the noble fir (8.2) and coastal Douglas-fir (7.2) models than the oak models, with the next greatest posterior mean in the black oak model (2.2). There was less variation in MCMC samples of σ_v from the oak models than the conifer models, which had wider equal-tailed 90% credible intervals for the posterior mean. Additional summaries of the posterior densities for ρ, σ_z, σ_v, and the components of $\boldsymbol{\beta}$ and $\boldsymbol{v}$ are also presented in Appendix S1: Section S4.

Species–climate relationships

Regression coefficients associated with quadratic terms had posterior means that were either significantly negative or not significantly different from zero (i.e., nonsignificant). Nonsignificant coefficients occurred in the blue oak (tmin-coldM, ppt-wetQ, and ppt-warmQ, all with negative posterior means) and white oak (ppt-warmQ, negative; tmax-warmM and ppt-wetQ, positive) models. Only tmin-coldM in the blue oak model had nonsignificant coefficients for both linear and quadratic terms.

Presented in Figure 3 are the fitted species response curves (a–c) for coastal Douglas-fir and the distribution of optimal conditions (d–e) estimated from the response curves; similar figures for the other four species are included in Appendix S1: Section S5. Optimal conditions were not estimated for gdd5 because only a linear term was considered for this covariate (Equation 17). The number of response curves from which optimal conditions could be estimated is shown in Table 4 for all species and the distribution of optimal conditions for coastal Douglas-fir is shown in Figure 3d (tmean-wetQ) and Figure 3e (the bivariate relationship of tmean-warmQ and ppt-warmQ, hereafter abbreviated as tmean-warmQ & ppt-warmQ).

For coastal Douglas-fir, all MCMC samples fit convex unimodal response curves for the relationships with tmean-wetQ (Figure 3b) and with tmean-warmQ & ppt-warmQ (Figure 3c). The mode of optimal tmean-wetQ conditions was 4.9°C, with 90% of the estimated optima between 4.1 and 6.2°C (Table 4). The mode of optimal tmean-warmQ & ppt-warmQ conditions was 21.1°C and 210.9 mm, which was estimated from 80% of MCMC samples (i.e., the 1592 samples that fit convex unimodal response curves with maxima within the climatic extremes of the current or future climate data sets; Table 4). Although 62% of MCMC samples fit sigmoidal-increasing response curves to gdd5 (Figure 3a), this covariate was not significant in coastal Douglas-fir's model.

All MCMC samples for noble fir and black oak fit convex unimodal response curves for all climate relationships involving quadratic terms. For black oak's relationship with gdd5 (which was not significant in the model), 69% of MCMC samples fit sigmoidal-decreasing response curves. All climate relationships for blue oak and white oak had at least one nonsignificant quadratic term (e.g., ppt-wetQ in white oak's relationship with tmean-wetQ & ppt-wetQ). Consequently, some MCMC samples fit concave unimodal response curves to univariate relationships or saddled response surfaces to bivariate relationships (i.e., concave with respect to the climate covariate with a nonsignificant quadratic term and convex with respect to the other covariate). However, within the range of climate conditions within which the species was observed (i.e., present based on FIA plot data), such response curves were generally sigmoidal or flat. Approximately half of the fitted response curves for white oak were concave unimodal for tmax-warmM (54%) or saddled for tmean-wetQ &

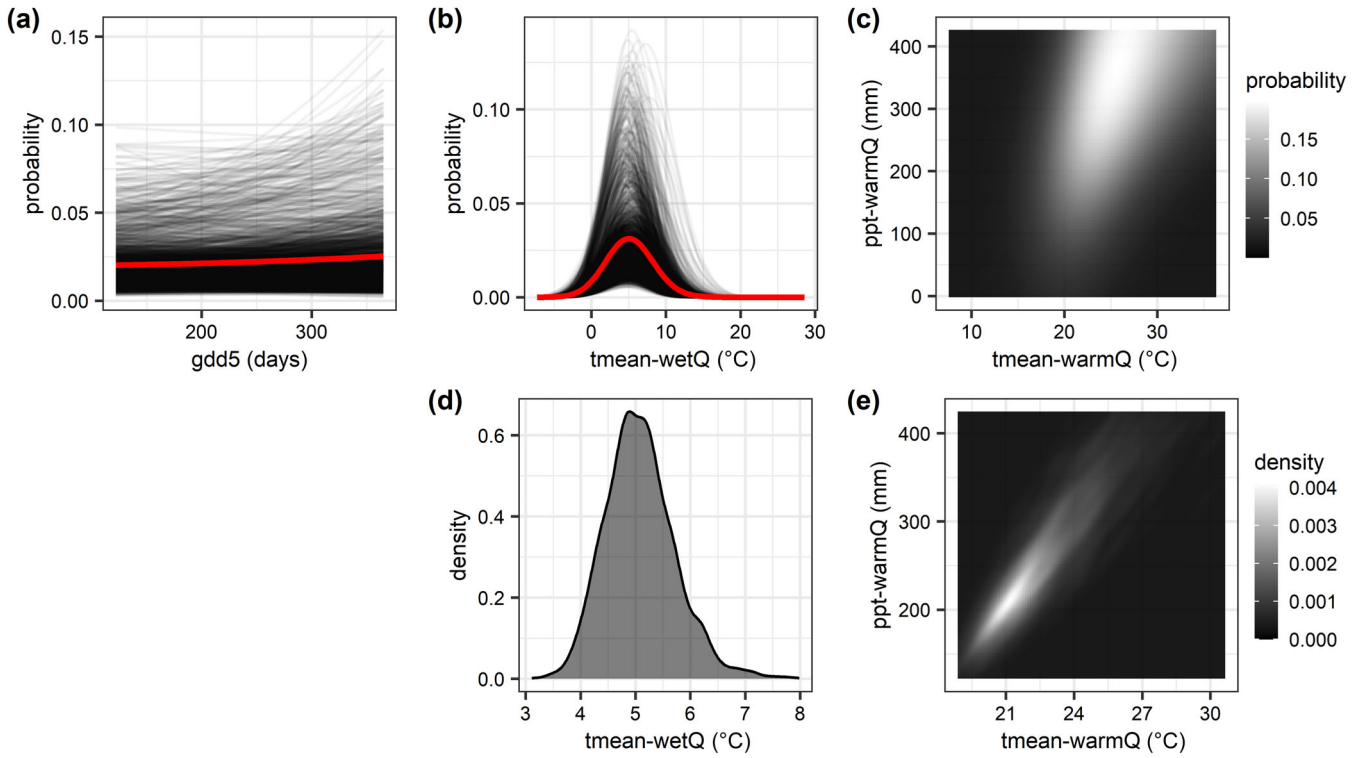

FIGURE 3 Fitted species response curves (a–c) and the distribution of optimal conditions (d–e) for coastal Douglas-fir to growing degree-days (gdd5; a), mean temperature of wettest quarter (tmean-wetQ; b, d), and the bivariate relationship of precipitation and mean temperature of warmest quarter (ppt-warmQ & tmean-warmQ, respectively; c, e). For the univariate relationships (a–b), response curves fit by individual Markov chain Monte Carlo samples are shown as gray lines and the mean of these 2000 response curves is shown in red. For the bivariate relationship in (c), only the mean of the 2000 response surfaces is shown (variation in these surfaces is included in Appendix S1: Section S5). In (d–e), a kernel density estimator was used to smooth over the optima of response curves from which optimal conditions could be estimated (i.e., 2000 in d and 1592 in e; Table 4).

TABLE 4 Summary statistics of optimal climate conditions based on fitted species response curves, including the number of Markov chain Monte Carlo (MCMC) samples that resulted in a response curve with an optimum (*N*), the maximum density or mode of those optima (mode), and, for univariate relationships, the 5th and 95th percentiles (pctl.) of the optima for noble fir (ABPR), coastal Douglas-fir (PSMEM), blue oak, (QUDO), white oak (QUGA4), and black oak (QUKE).

Species	Climate relationship	*N*	Mode	5th pctl.	95th pctl.
ABPR	tmean-warmQ & ppt-warmQ	1998	(13.4°C, 251.4 mm)		
PSMEM[a]	tmean-wetQ	2000	4.9°C	4.1°C	6.2°C
	tmean-warmQ & ppt-warmQ	1592	(21.2°C, 210.9 mm)		
QUDO	ppt-warmQ[b]	446	6 mm	1.2 mm	20.2 mm
	tmin-coldM[c]	1463	−0.2°C	−9.4°C	1.0°C
	tmean-wetQ & ppt-wetQ[b]	1607	(4.3°C, 615.9 mm)		
QUGA4	tmax-warmM[b]	558	38.4°C	34.9°C	53.1°C
	tmean-wetQ & ppt-wetQ[b]	463	(0.4°C, 610.6 mm)		
	tmean-warmQ & ppt-warmQ[b]	1016	(19.4°C, 28.8 mm)		
QUKE[a]	tmax-warmM	2000	34.1°C	33.1°C	37.7°C
	tmean-wetQ & ppt-wetM	2000	(5.1°C, 255.2 mm)		

Note: Optimal conditions were only estimated from MCMC samples that fit convex unimodal response curves with maxima within the climatic extremes of the current or future climate data sets.

[a]Optimal climate conditions were not estimated for gdd5.

[b]Quadratic term associated with this covariate was not significant in the model.

[c]No coefficients corresponding to this covariate were significant in the model.

ppt-wetQ (52%). Convex unimodal response curves were fit by the majority of MCMC samples for blue oak to ppt-warmQ (66%), tmin-coldM (80%), and tmean-wetQ & ppt-wetQ (95%), and for white oak to tmean-warmQ & ppt-warmQ (85%). For bivariate relationships, both species had a convex unimodal response to mean temperature covariates in all MCMC samples.

Between species, the mode of optimal tmean-wetQ & ppt-wetQ conditions was slightly warmer and wetter for blue oak than white oak (Table 4). The mode of optimal tmean-warmQ & ppt-warmQ conditions was cooler and wetter for noble fir than coastal Douglas-fir or white oak, and cooler and drier for white oak than coastal Douglas-fir. The estimated optimal tmax-warmM conditions were 4.3°C warmer for white oak than black oak.

Mean-prediction and uncertainty maps

For all species and under all future climate scenarios, the location of climatically suitable habitat generally shifted upwards in elevation or northward in latitude from the current mean-predictions as lower elevation or more southernly latitudes became less suitable (Figure 4). This trend held for coastal Douglas-fir for which the upward and northward movement of suitable habitat became more pronounced as future climate scenarios increased in severity (Figures 4 and 5); that is, from an intermediate emission pathway and a median climate projection (RCP 4.5 CCSM4) to a higher emission pathway and generally warmer climate projection (RCP 8.5 HadGEM2-ES). Future prediction uncertainty decreased for coastal Douglas-fir in the foothills of the Sierra Nevada mountains, where mean-predictions were projected to decrease, as well as in parts of the northern Cascade Range (hereafter, Cascades), where mean-predictions were projected to increase (Figure 5). Conversely, prediction uncertainty increased for future scenarios in parts of northern California and western Oregon where mean-predictions were projected to decrease. As expected, prediction uncertainty was generally lowest where there were many neighboring FIA plots without an observed presence; for coastal Douglas-fir, this can be seen in the foothills of the eastern Cascades in Oregon, the Modoc Plateau, and the southern Sierra Nevada (Figure 5).

For noble fir and black oak, elevation had a stronger impact on changes to climatically suitable habitat than latitude (Figure 4). Mean-predictions for noble fir substantially decreased under all four future scenarios as did prediction uncertainty (Appendix S1: Figure S14). For black oak, mean-predictions and uncertainty both generally increased at higher elevations in the Sierra Nevada, Northern Coast Ranges, and Klamath Mountains (Appendix S1: Figure S17). As the severity of future climate scenarios increased, mean-predictions and uncertainty for black oak progressively decreased along the western and northern limits of Great Central Valley and at lower elevations on the west side of the Sierra Nevada.

For blue oak and white oak, there were both elevational and latitudinal shifts of climatically suitable habitat under the future scenarios (Figure 4). As future scenarios increased in severity, mean-predictions for blue oak progressively increased at higher elevations and northward into the Klamath Mountains and progressively decreased at lower elevations around the Great Central Valley (Appendix S1: Figure S15). Similarly, for blue oak, uncertainty progressively increased in northern California and at lower elevations around the Sierra Nevada. Uncertainty for blue oak progressively decreased around the southern Great Central Valley and the southern Mojave Desert, although there were also some areas of increased uncertainty within these locales. For white oak, mean-predictions decreased throughout most of California and the Columbia River Basin under all future scenarios, with few areas seeing increased mean-predictions under the most severe future climate scenario (Appendix S1: Figure S16). However, under both CCSM4 scenarios and to a lesser extent the RCP 4.5 HadGEM2-ES scenario, mean-predictions increased near the Cascades from the area to the east of Mt. Adams down through southern Oregon. Changes in future prediction uncertainty for white oak generally mimicked changes in mean-predictions, with increased uncertainty near the Cascades and decreased uncertainty elsewhere.

Climate change impacts on range

Summarized in Figure 6 are the posterior distributions of the projected change (in thousand square kilometers) and relative change (in percentage; i.e., change relative to the current range size estimate) in range size under the four future climate scenarios. The posterior distributions of range size under the current and future scenarios are shown in Figure 7 (left panel). Additional summaries for range size metrics are provided in Appendix S1: Section S3. Note that we hereafter report posterior means unless stated otherwise.

The range size of noble fir significantly decreased under all future climate scenarios (Figure 6). Range size by the 2080s was approximately 9200 km^2 under the mildest scenario (RCP 4.5 CCSM4) and less than 7 km^2 under the three more severe scenarios (Figure 7; Appendix S1: Table S4). Relative to the current range size estimate, the projected decrease in range size was 78.9%

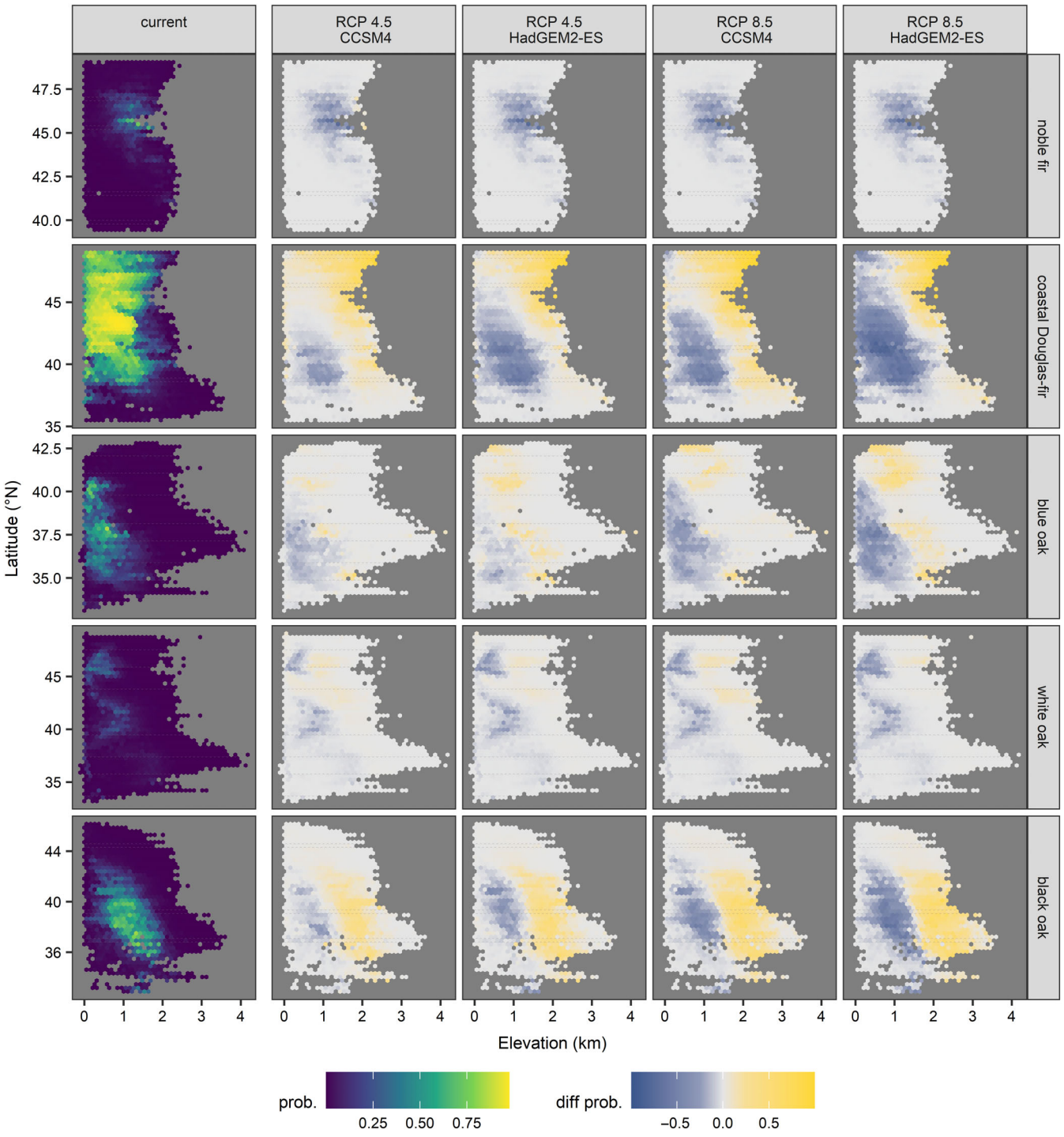

FIGURE 4 Mean-predictions (prob.) for the current scenario and change in mean-predictions (diff prob.) under the four future climate scenarios (visualized as future value − current value) by elevation (in kilometers) and latitude (°N). Areas where the mean-prediction increased under that future scenario are shown in yellow, areas that decreased are shown in blue, and areas with similar mean-predictions are shown in white. CCSM4, Community Climate System Model, version 4.0; HadGEM2-ES, Met Office Hadley Centre Global Environmental Model, version 2, Earth System; RCP, representative concentration pathway.

under the mildest scenario and nearly 100% under all other scenarios (Figure 6; Appendix S1: Table S3).

For both coastal Douglas-fir and white oak, range size significantly decreased under the three more severe climate scenarios, with no change in range size projected under the RCP 4.5 CCSM4 scenario. For coastal Douglas-fir, the smallest significant decrease in range size was 4.4% under the RCP 8.5 CCSM4 scenario and the

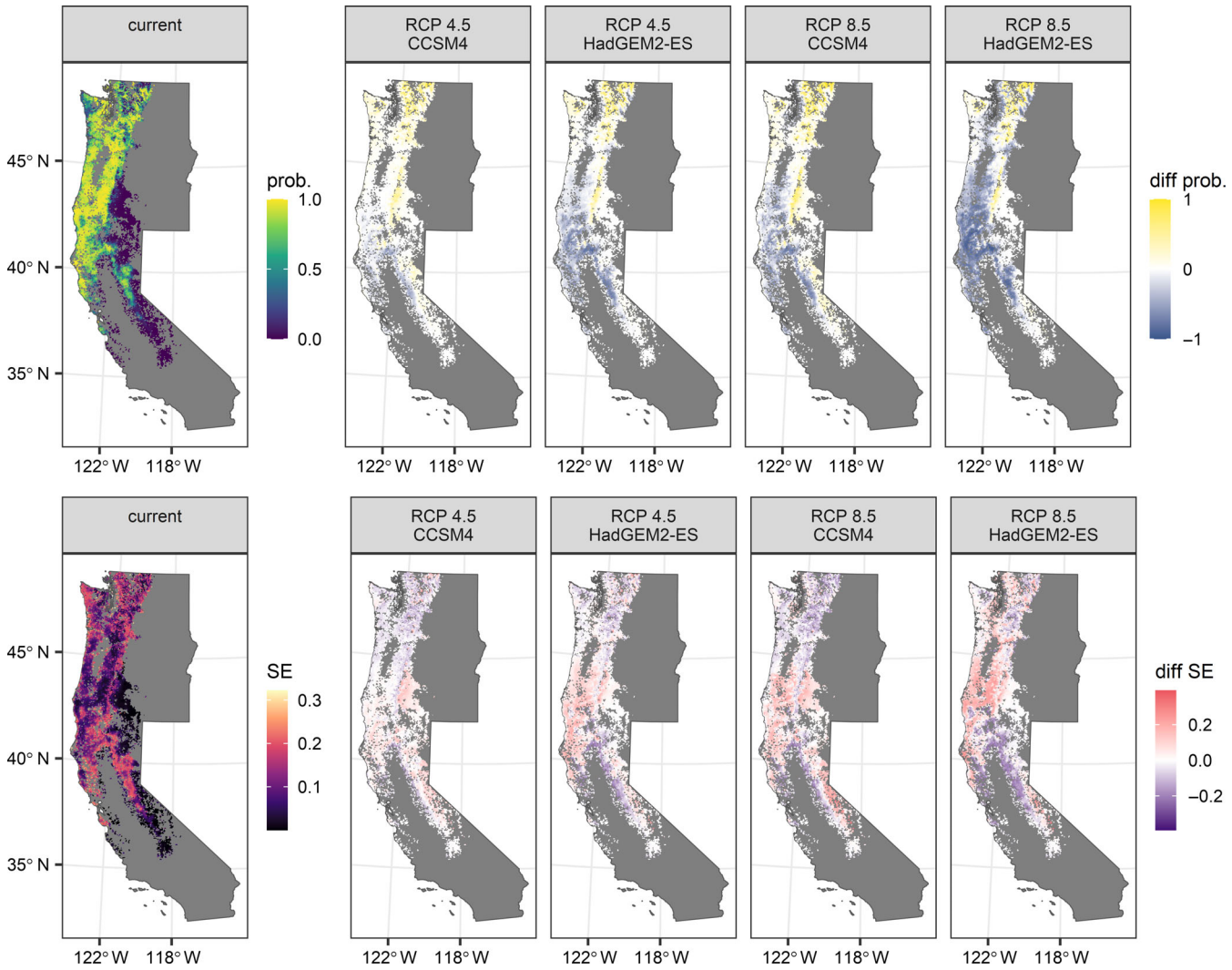

FIGURE 5 The current mean-predicted probability of climatically suitable habitat for coastal Douglas-fir (prob.), prediction uncertainty (SE), and the change in mean-predictions (diff prob.) and uncertainty (diff SE) under the four future climate scenarios (visualized as future value − current value). Areas where the mean-prediction increased under that future scenario are shown in yellow, areas that decreased are shown in blue, and areas with similar mean-predictions are shown in white. Similarly, areas that increased or decreased in uncertainty are shown in red or purple, respectively. CCSM4, Community Climate System Model, version 4.0; HadGEM2-ES, Met Office Hadley Centre Global Environmental Model, version 2, Earth System; RCP, representative concentration pathway.

largest decrease was 17.1% under the RCP 8.5 HadGEM2-ES scenario. Climate impacts were greater for white oak, with significant decreases in range size ranging from 26.8% (RCP 4.5 HadGEM2-ES) to 50.2% (RCP 8.5 HadGEM2-ES).

Unlike the other three species, range size for blue oak and black oak did not decrease under any future scenario. No significant change in range size was projected for blue oak, though credible intervals for posterior means were wide. Relative change in range size for blue oak varied from −0.8% (RCP 4.5 CCSM4) to 17.2% (RCP 8.5 HadGEM2-ES). Black oak's range size significantly increased under all future scenarios, with increases in range size between 17.0% (RCP 8.5 HadGEM2-ES) and 24.7% (RCP 8.5 CCSM4).

The trade-offs between range expansion and contraction (in thousand square kilometers) under the future climate scenarios are illustrated in the right panel of Figure 7. Posterior means and equal-tailed 90% credible intervals for the area (in thousand square kilometers) and relative area (in percentage; area relative to the current range size estimate) of range expansion, contraction, and persistence are included in Appendix S1: Table S5. In general, less contraction indicates that more of the range is projected to remain climatically suitable and persist under that future scenario.

Climatically suitable habitat for noble fir substantially decreased under all future climate scenarios, with no significant range expansion under any scenario (i.e., zero

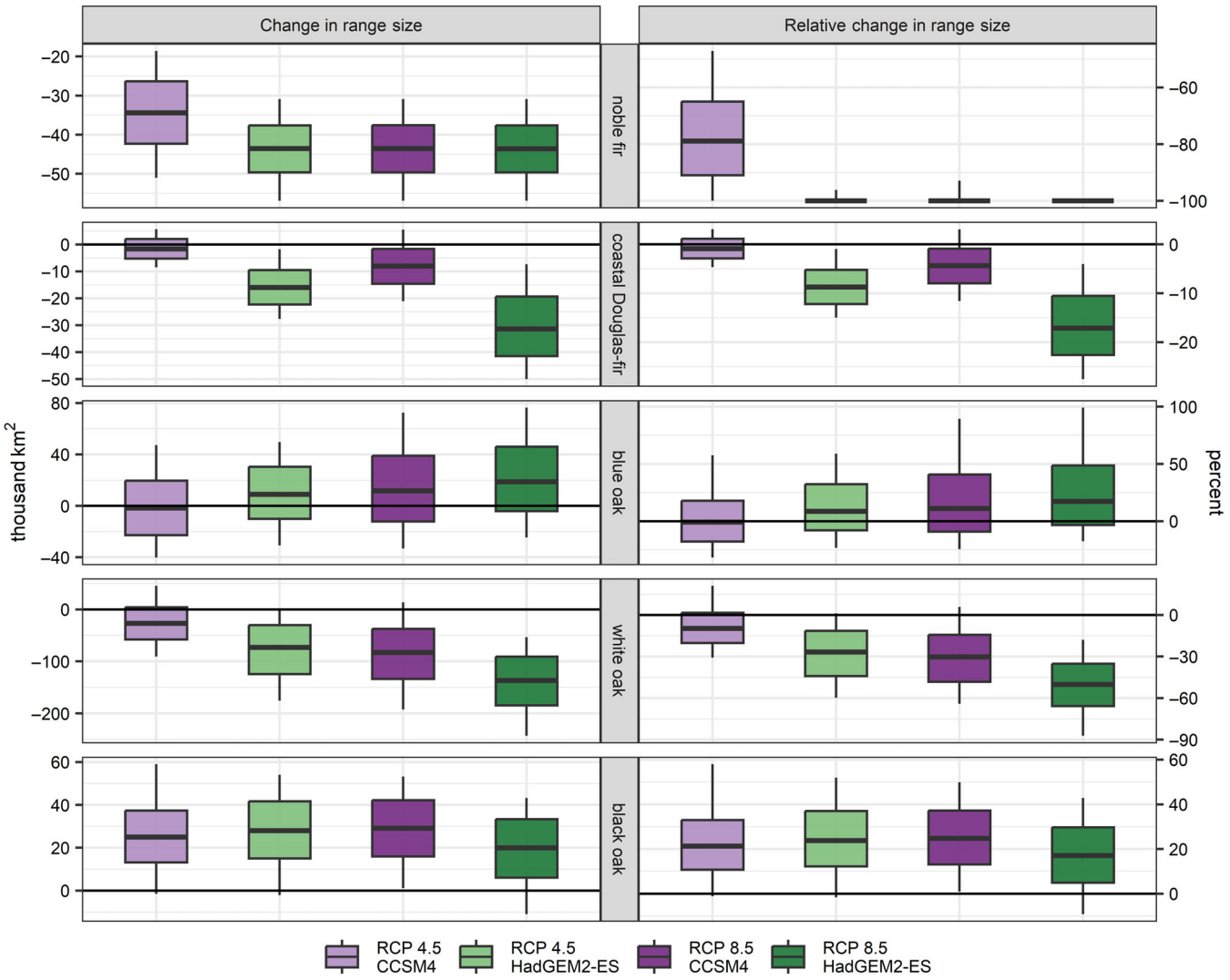

FIGURE 6 Box plot summaries for the posterior distributions of the change (in thousand square kilometers) and relative change (in percentage) in range size between the current and a future climate scenario's estimate based on the bivariate kernel density estimation method. Change is calculated as future value − current value and relative change is calculated as (future value − current value)/current value. Positive values indicate an overall increase in range size by the 2080s and negative values indicate a decrease. Box plot summaries include the minimum and maximum sample values (indicated by the lower and upper whiskers, respectively), the 5th and 95th percentile (the lower and upper hinges, respectively), and the posterior mean (middle line segment). The box plot hinges can be interpreted as an equal-tailed 90% credible interval for the posterior mean; the horizontal black line indicates a value of zero for reference. CCSM4, Community Climate System Model, version 4.0; HadGEM2-ES, Met Office Hadley Centre Global Environmental Model, version 2, Earth System; RCP, representative concentration pathway.

included in the credible interval for the relative area of range expansion). Expansion was approximately 400 km^2 under the mildest future scenario (RCP 4.5 CCSM4) and less than 1 km^2 for all other future scenarios. Although 20.3% of the current range was projected to remain climatically suitable under the RCP 4.5 CCSM4 scenario, there was no significant range persistence under the three more severe future scenarios.

For coastal Douglas-fir, expansion was generally less under the milder climate model (i.e., CCSM4 being generally milder with respect to warming than HadGEM2-ES) and contraction tended to be greater under the higher emissions pathway (RCP 8.5 being higher emissions than RCP 4.5). Across the future climate scenarios, between 81.6% (RCP 8.5 HadGEM2-ES) and 96.5% (RCP 4.5 CCSM4) of coastal Douglas-fir's current range was projected to remain climatically suitable. Nevertheless, even under the RCP 4.5 CCSM4 scenario, for which no significant change in range size was projected (Figure 6), approximately 6400 km^2 of coastal Douglas-fir's current range was still projected to become climatically unsuitable by the 2080s.

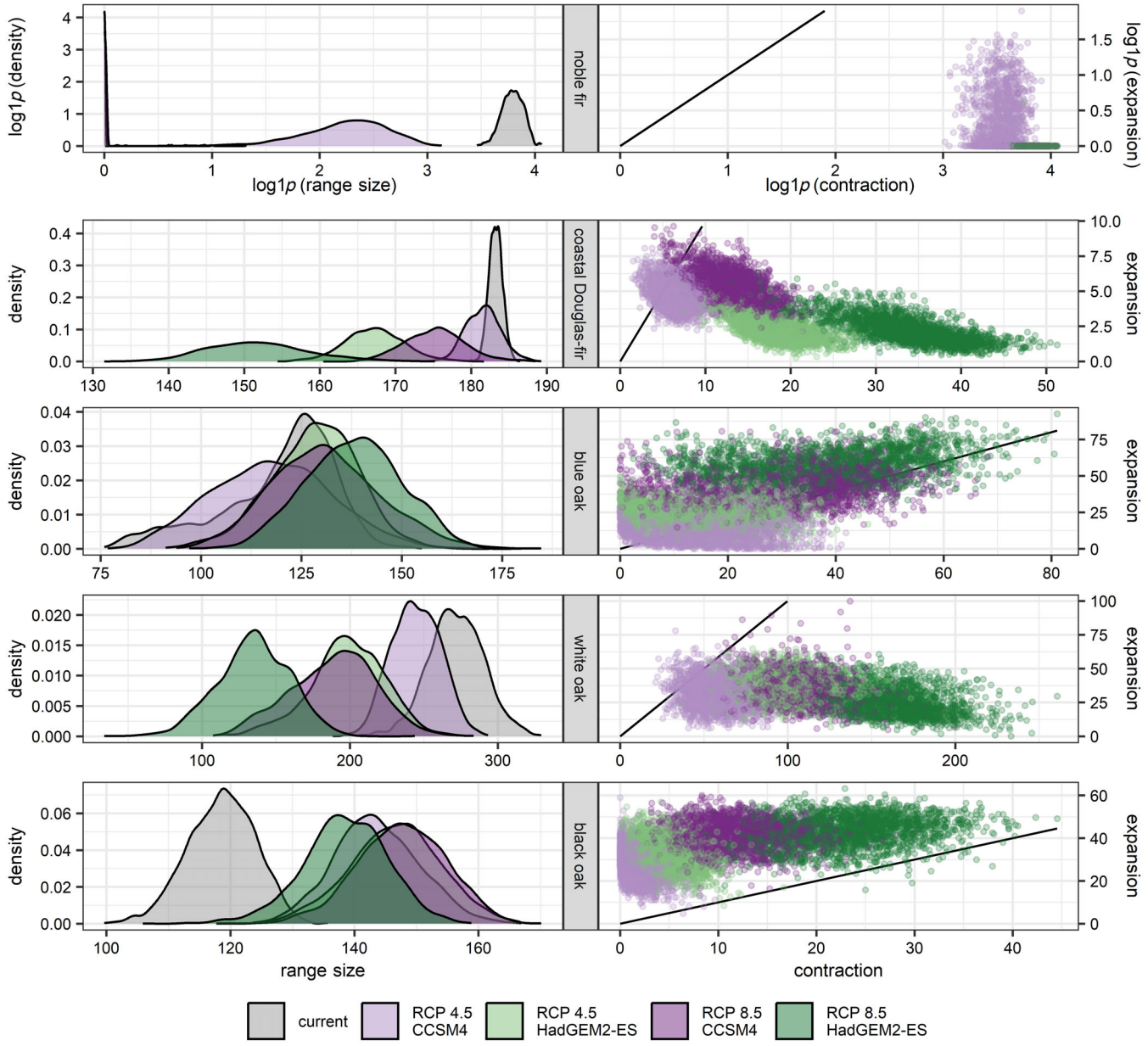

FIGURE 7 The posterior distribution of range size (in thousand square kilometers; left panel) and comparison of range expansion and contraction (in thousand square kilometers; right panel) for the current and four future climate scenarios. For visibility, axes for noble fir are visualized on the $\log1p(x) = \ln(x + 1)$ scale, while axes for all other species are untransformed. In the right panel, each point corresponds to an individual Markov chain Monte Carlo (MCMC) sample plotted by range expansion (area projected to become climatically suitable; area within the future range but not the current range) and range contraction (area projected to become climatically unsuitable; area within the current range but not the future range). Points clustered along the black line of equality between range expansion and contraction represent MCMC samples with similar range size estimates under the current and a future scenarios. CCSM4, Community Climate System Model, version 4.0; HadGEM2-ES, Met Office Hadley Centre Global Environmental Model, version 2, Earth System; RCP, representative concentration pathway.

For blue oak, no significant change in total range size was projected under any future scenario (Figure 6), but only between 68.5% (RCP 8.5 HadGEM2-ES) and 86.9% (RCP 4.5 HadGEM2-ES) of its current range was projected to remain climatically suitable by the 2080s. The greatest shift in blue oak's climatically suitable habitat was projected under the RCP 8.5 HadGEM2-ES scenario (based on both posterior means and the upper bound of 90% credible intervals), for which nearly 38,600 km^2 of the current range was projected to become unsuitable and almost 48,700 km^2 was projected to become suitable by the 2080s.

Under the RCP 4.5 CCSM4 scenario, white oak was projected to lose nearly 21,500 km^2 of climatically suitable habitat from its current range, despite no significant change in range size. There was greater variability among future scenarios in terms of range contraction than range expansion. Projected range expansion, contraction, and persistence were similar under the RCP 4.5 HadGEM2-ES and RCP 8.5 CCSM4 scenarios (overlapping 90% credible intervals).

As expected, based on results for black oak's range size (i.e., significant increase under all future scenarios), expansion tended to exceed contraction under all future climate scenarios (i.e., points above the line of equality between expansion and contraction in Figure 7). Posterior means for both expansion and contraction increased with increasing severity of the future climate scenario. Credible intervals for contraction area overlapped between future climate scenarios that were adjacent in severity. As with all other species, black oak's current range was projected to contract under all future climate scenarios. At least 1600 km^2 (RCP 4.5 CCSM4) but upwards of 23,300 km^2 (RCP 8.5 HadGEM2-ES) of black oak's current range was projected to become unsuitable by the 2080s.

DISCUSSION

Modeling approach

We projected climatically suitable habitat for five tree species by fitting spatial Bayesian hierarchical models with MCMC methods. The primary benefits of this modeling approach included the ability to quantify uncertainty, accommodate complex model forms with latent variables, and inspect ecological relationships that would have been unexaminable with more traditional methods. The approach allowed us to develop spatially informed relationships between current climate and species occurrence with strong predictive performance (AUC > 0.95). We found evidence of strong autocorrelation (posterior mean of $\rho > 0.97$) in all species-specific data sets and minimal remaining spatial autocorrelation after spatial dependency was incorporated through a CAR model (Moran's I model check within 0.04 of 0). Lastly, our modeling approach allowed us to incorporate climate information from areas where the species response was unobserved, which enabled us to obtain more realistic estimates of uncertainty along the forest/nonforest boundary. This was especially useful for species that commonly occur in conditions that bridge the forest/nonforest FIA designations (blue oak and white oak).

Fitting spatial Bayesian hierarchical models can be computationally prohibitive for large data sets. Accordingly, we implemented a variety of strategies from Ver Hoef et al. (2021) to speed up estimation, including sparse matrix calculations, simplifying density calculations for Metropolis–Hastings acceptance weights, and using lookup tables for inverse and determinate calculations of $\boldsymbol{\Sigma}_\theta$ based on different values of ρ. When data sets included unobserved response data (i.e., blue oak and white oak), we also increased the sampling rates for $\boldsymbol{z}_o$ and $\boldsymbol{z}_u$ to speed up convergence. Although these modifications substantially improved computational and temporal efficiency, other unique features of our data sets likely contributed to a slower model-fitting process than traditional modeling approaches. Data features that may contribute to longer run times likely include a binary response, low observed prevalence, and many latent (spatial) variables for some species. Consideration of these data features and the availability of computational resources will be important when weighing the advantages and disadvantages of this modeling approach for future applications.

Our predictions for future climate scenarios use the spatial patterning (error structure) observed under the current climate. By using the spatial random effects ($\boldsymbol{z}$) for future predictions, we assumed that the current spatial patterning would hold into the future. We believe this assumption is reasonable, because of the long-lived, sessile nature of our focal species (trees) and our projection window of less than 100 years. While it is debatable whether these exact $\boldsymbol{z}$ values will hold into the future, this approach has the advantage of retaining the spatial patterning of over- and underprediction present in the current data set. Another possible approach is simulating random errors from the fitted CAR model. Simulating random errors from the CAR model has the advantage of acknowledging autocorrelation in predictions but would "shuffle" areas of over- and underprediction. This "shuffle" has a greater potential to result in an unrealistic error patterning under future scenarios than our chosen method.

Multiple sources of uncertainty are inherently tied to any predictions of a species' current or future habitat. In this study, the characterization of both covariate and prediction uncertainty was made possible by our MCMC model-fitting approach. This included the ability to develop credible intervals for parameters, visualize uncertainty of response curves, and map both current and future prediction uncertainty. We were also able to obtain samples from the posterior distribution of any statistic subsequently calculated on our MCMC samples from the model's posterior distribution, which enabled us to obtain credible intervals for that statistic, perform significance tests, and provide uncertainty estimates of change under a future climate scenario. Many of these

methods for characterizing model and estimate uncertainty are not possible with traditional species distribution modeling methods and are a unique advantage of hierarchical models fit with MCMC methods.

One of the goals of this project was to provide a detailed assessment of potential climate change impacts on these five species for planning and management efforts and to demonstrate how uncertainty can be characterized in climate change studies. When projections of future habitat are of interest, the choice of emission pathway, AOGCM, and time period will all impact habitat projections. Because there is inherent uncertainty in forecasts of future climate, we presented the results for two emission pathways each interpreted by two AOGCMs for the 2080s.

Model interpretation and species–climate relationship

We interpreted model predictions as the probability of climatically suitable habitat rather than the species occurrence, a distinction that has been discussed elsewhere in the literature (e.g., Elith & Leathwick, 2009; Rehfeldt et al., 2014a). Although a location may be predicted to become suitable for a species, it is possible that the species will not be able to occupy those locations because of biotic or abiotic factors not considered in this analysis (e.g., dispersal rates, disturbance, competition). Similarly, unaccounted-for factors may also influence mortality in locations projected to become unsuitable and widespread mortality of species will likely lag behind changes in habitat suitability as trees are long-lived and sessile. Furthermore, in locations where climatically suitable habitat is projected to persist, a species may not be able to occupy those locations, because of differences in adaptational lags between local populations (Rehfeldt et al., 2014a).

The species' response curves estimated by our models mostly matched the convex unimodal shape we expected (as reviewed in the *Introduction*). For some covariates in the blue oak and white oak models, nonsignificant quadratic terms resulted in response curves that were not consistently convex unimodal. However, these response curves still agreed with theory when examined within the climate conditions in which the species was observed. The results for blue oak and white oak emphasize the need for careful model interpretation. For these species, unaccounted-for factors may have influenced the species–climate relationships captured by the modeling data sets. Our data sets lacked observations for these species in conditions with low (less than 10%) canopy cover or stocking, locations hosting the hottest and driest conditions in which these species grow. Additionally, the influence of competition and historical management practices on the current distributions of blue oak and white oak (Gould et al., 2011; McDonald, 1990; Stein, 1990) is also likely reflected in the estimated shape of response curves and, consequently, optimal climate conditions.

For most covariates, the mode of optimal conditions was within the observed range of conditions for each species. There were a few exceptions related to quarterly precipitation covariates (i.e., ppt-wetQ, ppt-warmQ), for which the mode was estimated as nearly double the observed maximum for the species: ppt-warmQ in the noble fir and coastal Douglas-fir models, and ppt-wetQ in the blue oak and white oak models. The climate of the PNW is characterized by a dry period from late spring to mid-autumn, which aligns with the growing season (Franklin & Dyrness, 1973). Because plant moisture stress is high during warm months (Waring & Franklin, 1979), it is not unexpected that the models for noble fir and coastal Douglas-fir would identify wetter ppt-warmQ (precipitation during the warmest quarter) conditions as ideal even though such conditions may not be realizable (Franklin, 1990; Hermann & Lavender, 1990). Similarly for blue oak and white oak, the wetter ppt-wetQ (precipitation during the wettest quarter) conditions identified as ideal by the models may represent sites at which these species are outcompeted. Although the high drought tolerance of these oaks allows them to occupy exposed or droughty sites, they are often outcompeted by conifers (and, for blue oak, other oak species) at more favorable sites, such as moist sites with fertile soils (McDonald, 1990; Stein, 1990).

Impact of climate change on suitable habitat

The results of this study affirm that important tree species of the PNW will be impacted by projected changes in climate by the end of this century. We found that the location of climatically suitable habitat would shift by the 2080s for all species considered in this study. The percent of current habitat projected to become unsuitable varied by species, with some species and climate projections indicating that future range expansion would not offset contraction.

Some broad trends were consistent for species across future climate scenarios. By the 2080s, there was a general upward elevational or northward latitudinal movement of suitable habitat for all species. Such elevational or latitudinal shifts are a common finding in climate change studies of tree species distributions (Iverson et al., 2008; McKenney et al., 2007). For most species in our analysis, projected shifts in suitable habitat were the

result of both range expansion and contraction. Although the amount of range contraction varied between species and future scenarios, all species were projected to experience some loss of habitat from their current range. Mortality rates in the areas becoming climatically unsuitable (i.e., contraction) will generally outpace immigration rates in areas becoming suitable (i.e., expansion), even when the total amount of suitable habitat remains constant (Rehfeldt et al., 2014a). Consequently, near-term realizations of this shift in climatically suitable habitat may appear as a loss of habitat and a decrease in range size.

Climate change impacts were projected to be the most damaging for noble fir. Noble fir was the only species that was not projected to gain newly suitable habitat under a future climate scenario. By the 2080s, suitable habitat for this species was projected to reduce by at least 78.9% under all four climate scenarios. These findings agree with other studies that have identified noble fir as highly vulnerable to climate change (Case & Lawler, 2016; Crookston et al., 2010; Devine et al., 2012; McKenney et al., 2007). Although suitable habitat for noble fir may exist in the 2080s within microrefugia or at higher elevations not captured by our data set, it is uncertain how quickly high-elevation tree species will be able to colonize alpine environments (Bell et al., 2014). Therefore, climate change poses a serious threat to noble fir, whose current habitat already occurs in isolated patches or along the western slope and crest of the Cascades.

For coastal Douglas-fir, losses in climatically suitable habitat were primarily projected at lower elevations to the south and west of the current range, with habitat gains projected for the eastside of the Cascades. Although we projected a significant decrease in range size under three of the climate scenarios, these estimates are specific to our study area and do not address impacts on the Canadian portion of coastal Douglas-fir's distribution, where the species has been projected to expand (Mathys et al., 2017; Rehfeldt et al., 2014a). However, within our study area, our projections agree with other climate change studies (Gray & Hamann, 2013; Mathys et al., 2017; Rehfeldt et al., 2014a). Similar to Rehfeldt et al. (2014a), the lower climatic suitability we projected around Puget Sound is likely a reflection of the lack of climate analogs in the current data set, rather than true unsuitability of this environment for coastal Douglas-fir. Nevertheless, we found that up to 18.4% of coastal Douglas-fir's current habitat within the PNW was projected to become climatically unsuitable by the 2080s.

We projected that nearly a third of suitable habitat for forest land blue oak in the 2080s will exist where blue oak is not currently present, with much of this new habitat to the north where conifer species are dominant. These findings agree with other climate change assessments of blue oak (Brown et al., 2018; Kueppers et al., 2005; Serra-Diaz et al., 2014), including decreases in habitat suitability that will primarily occur in locations to the south of blue oak's range surrounding the Great Central Valley. These areas with projected lower suitability agree with estimates by Brown et al. (2018) of 2015 dieback from the 2012 to 2015 California drought, which is notable as our data set predates this drought event. In California, where blue oak is endemic, the risk of drought is expected to increase as warmer temperatures lead to greater evaporative demand (Cook et al., 2015), even in some areas where increased cold season precipitation is expected (Neelin et al., 2013).

Second only to noble fir, white oak was projected to undergo substantial decrease in climatically suitable habitat from climate change. Although not unexpected, our current predictions of climatically suitable habitat were somewhat broader than the current observed presence of this species, including higher suitability throughout the Columbia Basin. This is likely the result of factors associated with the contemporary decline of white oak, such as changes in land use and fire exclusion on wetter sites, which can promote conifer invasion (Hahm et al., 2018). However, white oak tends to have greater drought tolerance relative to its competitors (Hahm et al., 2018). Pellatt et al. (2012) also predicted broader current suitability for white oak when predictions were developed for the northern portion of this species range. Like Pellatt et al. (2012), we projected that the probability of climatically suitable habitat would increase by the 2080s to the east of the Cascades. However, unlike Pellatt et al. (2012), we did not see the same increase in white oak habitat for southwestern Oregon that they projected for the 2080s. This could be the result of differences in our data sets (i.e., our inclusion of white oak observations from the southern portion of the species' range). Although some areas were projected to become climatically suitable under all scenarios, approximately 58,700–161,700 km^2 of forest land white oak's current range was projected to become unsuitable.

Unlike the other four species, we projected that the amount of climatically suitable habitat for black oak would significantly increase by the 2080s under all but the most severe future climate scenario. Similarly, Lenihan et al. (2008) projected an expansion of hardwoods, including black oak, in California's mixed evergreen forests by the 2080s. Despite these habitat gains, we projected that approximately 1600–23,300 km^2 of black oak's current range would become unsuitable. Because black oak is a poor competitor on moist sites and becomes increasingly shade intolerant with age, mature black oaks tend to dominate harsh, dry soil sites that are vulnerable to moisture stress (appendix 8 of Devine

et al., 2012, Long et al., 2016). Recent trends (1991–2016) from California and Oregon found a slight decline in the basal area (cross-sectional area) of large black oak trees to be mainly associated with fire-related mortality (Long et al., 2018). In addition to competition, other threats, such as *Phytophthora ramorum* (the sudden oak death pathogen) in the more cool and humid northwestern extent of black oak's contemporary range, will temper what sites black oak can occupy in the future (Long et al., 2016). Given the elevated cultural and ecological importance of mature, large black oak trees (Long et al., 2017), the impact of climate change on this species may be considerable.

CONCLUSION

Rapid changes in climate are projected to shift the location of climatically suitable habitat for important tree species in the PNW by the 2080s. Northward latitudinal or upward elevational shifts in suitable habitat were projected for all species. However, the most damaging impacts were projected for the high-elevation species examined in this study, noble fir, with a near-total loss of climatically suitable habitat under most scenarios. Overall reductions in suitable habitat were also projected for the portion of coastal Douglas-fir and Oregon white oak's ranges within the contiguous United States. Although gains in climatically suitable habitat were projected to meet or exceed losses for blue oak and black oak, other threats to these species exist. As global and local climates continue to change, successful management of natural resources like forests will continue to depend on an iteratively updated understanding of the potential impacts of new climate projections on species distributions. In addition to obtaining predictions, the spatial Bayesian hierarchical models fit in this study allowed for uncertainty surrounding current and future predictions and estimates of change to be characterized. These findings provide a detailed assessment of the relative pressures these species will face in tracking climatically suitable habitat within this century.

ACKNOWLEDGMENTS

This work was supported in part by the U.S. Department of Agriculture (USDA), Forest Service. The findings and conclusions in this publication are those of the authors and should not be construed to represent any official USDA or U.S. Government determination or policy. This article was prepared in part by employees of the USDA Forest Service as part of official duties and is therefore in the public domain. This research was also supported in part by an appointment to the USDA Forest Service Research Participation Program administered by the Oak Ridge Institute for Science and Education (ORISE) through an interagency agreement between the U.S. Department of Energy (DOE) and the USDA. ORISE is managed by Oak Ridge Associated Universities (ORAU) under DOE contract number DE-SC0014664. All opinions expressed in this paper are the author's and do not necessarily reflect the policies and views of USDA, DOE, or ORAU/ORISE.

CONFLICT OF INTEREST STATEMENT

The authors declare that the research was conducted in the absence of any commercial or financial relationships that could be construed as a potential conflict of interest.

DATA AVAILABILITY STATEMENT

The R code used in this analysis (Kralicek, 2023) is available from Zenodo: https://doi.org/10.5281/zenodo.7586213. Data supporting this research are sensitive and are not available publicly. While imprecise location (fuzzed) coordinates for the Forest Inventory and Analysis (FIA) Program's field data are publicly available (https://apps.fs.usda.gov/fia/datamart/datamart.html), precise location coordinates are confidential. However, the data used in this research were internally archived within the FIA program's file structure by Karin Kralicek, such that someone obtaining permission to access these data could replicate the analysis. Requests to access precise location FIA data sets for the PNW should be directed to the Pacific Northwest FIA (PNW-FIA) program at pnw_iram@fs.usda.gov or by visiting https://www.fia.fs.usda.gov/about/about_us/#questions-requests.

ORCID

Karin Kralicek https://orcid.org/0000-0003-0793-321X

REFERENCES

Akaike, H. 1973. "Information Theory and an Extension of the Maximum Likelihood Principle." In *Second International Symposium on Information Theory*, edited by B. N. Petrov and F. Csäki, 267–81. Budapest: Akademiai Kiàdo.

Araújo, M. B., and A. T. Peterson. 2012. "Uses and Misuses of Bioclimatic Envelope Modeling." *Ecology* 93: 1527–39. https://doi.org/10.1890/11-1930.1.

Austin, M. 2007. "Species Distribution Models and Ecological Theory: A Critical Assessment and some Possible New Approaches." *Ecological Modelling* 200: 1–19. https://doi.org/10.1016/j.ecolmodel.2006.07.005.

Bell, D. M., J. B. Bradford, and W. K. Lauenroth. 2014. "Mountain Landscapes Offer Few Opportunities for High-Elevation Tree Species Migration." *Global Change Biology* 20: 1441–51. https://doi.org/10.1111/gcb.12504.

Besag, J. 1974. "Spatial Interaction and the Statistical Analysis of Lattice Systems." *Journal of the Royal Statistical Society: Series B (Methodological)* 36: 192–236.

Blatner, K. A., P. J. Cohn, and R. D. Fight. 2010. "Returns from the Management of Noble Fir Stands for Bough Production and Sawtimber." *Western Journal of Applied Forestry* 25: 68–72. https://doi.org/10.1093/wjaf/25.2.68.

Brown, B. J., B. C. McLaughlin, R. V. Blakey, and N. Morueta-Holme. 2018. "Future Vulnerability Mapping Based on Response to Extreme Climate Events: Dieback Thresholds in an Endemic California Oak." *Diversity and Distributions* 24: 1186–98. https://doi.org/10.1111/ddi.12770.

Burrill, E. A., A. M. DiTommaso, J. A. Turner, S. A. Pugh, J. Menlove, G. Christiansen, C. J. Perry, and B. L. Conkling. 2021. *The Forest Inventory and Analysis Database: Database Description and User Guide Version 9.0.1 for Phase 2*. Washington DC: USDA Forest Service. http://www.fia.fs.usda.gov/library/database-documentation/.

Case, M. J., and J. J. Lawler. 2016. "Relative Vulnerability to Climate Change of Trees in Western North America." *Climatic Change* 136: 367–79. https://doi.org/10.1007/s10584-016-1608-2.

Chacón, J. E., and T. Duong. 2010. "Multivariate Plug-in Bandwidth Selection with Unconstrained Pilot Bandwidth Matrices." *TEST* 19: 375–98. https://doi.org/10.1007/s11749-009-0168-4.

Cleland, D. T., J. A. Freeouf, J. E. Keys, G. J. Nowacki, C. A. Carpenter, and W. H. McNab. 2007. *Ecological Subregions: Sections and Subsections for the Conterminous United States*. General Technical Report WO-76D. Washington DC: USDA Forest Service. https://www.fs.usda.gov/treesearch/pubs/48672.

Conn, P. B., D. S. Johnson, P. J. Williams, S. R. Melin, and M. B. Hooten. 2018. "A Guide to Bayesian Model Checking for Ecologists." *Ecological Monographs* 88: 526–42. https://doi.org/10.1002/ecm.1314.

Cook, B. I., T. R. Ault, and J. E. Smerdon. 2015. "Unprecedented 21st Century Drought Risk in the American Southwest and Central Plains." *Science Advances* 1: e1400082. https://doi.org/10.1126/sciadv.1400082.

Cressie, N. 1993. *Statistics for Spatial Data*, Revised ed. New York: Wiley.

Cressie, N., C. A. Calder, J. S. Clark, J. M. Ver Hoef, and C. K. Wikle. 2009. "Accounting for Uncertainty in Ecological Analysis: The Strengths and Limitations of Hierarchical Statistical Modeling." *Ecological Applications* 19: 553–70. https://doi.org/10.1890/07-0744.1.

Crookston, N. L., G. E. Rehfeldt, G. E. Dixon, and A. R. Weiskittel. 2010. "Addressing Climate Change in the Forest Vegetation Simulator to Assess Impacts on Landscape Forest Dynamics." *Forest Ecology and Management* 260: 1198–211. https://doi.org/10.1016/j.foreco.2010.07.013.

Devine, W., C. Aubry, A. Bower, J. Miller, and N. Maggiulli Ahr. 2012. *Climate Change and Forest Trees in the Pacific Northwest: A Vulnerability Assessment and Recommended Actions for National Forests*. Olympia, WA: USDA Forest Service, Pacific Northwest Research Station. http://ecoshare.info/projects/ccft.

Duong, T. 2020. "Ks: Kernel Smoothing." R Package Version 1.11.7. https://CRAN.R-project.org/package=ks.

Elith, J., and J. R. Leathwick. 2009. "Species Distribution Models: Ecological Explanation and Prediction across Space and Time." *Annual Review of Ecology, Evolution, and Systematics* 40: 677–97. https://doi.org/10.1146/annurev.ecolsys.110308.120159.

Franklin, J. F. 1990. "*Abies procera* Rehd. Noble Fir." In *Silvics of North America: Vol. 1. Conifers. Agriculture Handbook 654*, edited by R. M. Burns and B. H. Honkala, 80–7. Washington DC: USDA Forest Service.

Franklin, J. 2009. *Mapping Species Distributions: Spatial Inference and Prediction*. Cambridge: Cambridge University Press.

Franklin, J. F., and C. T. Dyrness. 1973. *Natural Vegetation of Oregon and Washington*. General Technical Report PNW-GTR-008. Portland, OR: USDA Forest Service, Pacific Northwest Research Station.

Fuchs, M. A. 2001. *Towards a Recovery Strategy for Garry Oak and Associated Ecosystems in Canada: Ecological Assessment and Literature Review*. Technical Report GBEI/EC-00-030. Environment Canada, Canadian Wildlife Service, Pacific and Yukon Region.

Garfin, G., G. Franco, H. Blanco, A. Comrie, P. Gonzalez, T. Piechota, R. Smyth, and R. Waskom. 2014. "Chapter 20: Southwest." In *Climate Change Impacts in the United States: The Third National Climate Assessment*, edited by J. M. Melillo, T. C. Richmond, and G. W. Yohe, 462–86. Washington DC: US Global Change Research Program. https://doi.org/10.7930/J04Q7RWX.

Gelfand, A. E., and A. F. M. Smith. 1990. "Sampling-Based Approaches to Calculating Marginal Densities." *Journal of the American Statistical Association* 85: 398–409. https://doi.org/10.2307/2289776.

Gent, P. R., G. Danabasoglu, L. J. Donner, M. M. Holland, E. C. Hunke, S. R. Jayne, D. M. Lawrence, et al. 2011. "The Community Climate System Model Version 4." *Journal of Climate* 24: 4973–91. https://doi.org/10.1175/2011JCLI4083.1.

Gilks, W. R., S. Richardson, and D. J. Spiegelhalter. 1996. "Introducing Markov Chain Monte Carlo." In *Markov Chain Monte Carlo in Practice*, edited by W. R. Gilks, S. Richardson, and D. J. Spiegelhalter, 1–19. New York: Chapman & Hall/CRC.

Gitzen, R. A., J. J. Millspaugh, and B. J. Kernohan. 2006. "Bandwidth Selection for Fixed-Kernel Analysis of Animal Utilization Distributions." *Journal of Wildlife Management* 70: 1334–44. https://doi.org/10.2193/0022-541X(2006)70[1334:BSFFAO]2.0.CO;2.

Gould, P. J., C. A. Harrington, and W. D. Devine. 2011. "Growth of Oregon White Oak (*Quercus garryana*)." *Northwest Science* 85: 159–71. https://doi.org/10.3955/046.085.0207.

Gray, L. K., and A. Hamann. 2013. "Tracking Suitable Habitat for Tree Populations under Climate Change in Western North America." *Climate Change* 117: 289–303. https://doi.org/10.1007/s10584-012-0548-8.

Gugger, P. F., S. Sugita, and J. Cavender-Bares. 2010. "Phylogeography of Douglas-Fir Based on Mitochondrial and Chloroplast DNA Sequences: Testing Hypotheses from the Fossil Record." *Molecular Ecology* 19: 1877–97. https://doi.org/10.1111/j.1365-294X.2010.04622.x.

Hahm, W. J., W. E. Dietrich, and T. E. Dawson. 2018. "Controls on the Distribution and Resilience of *Quercus garryana*: Ecophysiological Evidence of Oak's Water-Limitation Tolerance." *Ecosphere* 9: e02218. https://doi.org/10.1002/ecs2.2218.

Hanley, J. A., and B. J. McNeil. 1982. "The Meaning and Use of the Area under a Receiver Operating Characteristic (ROC) Curve." *Radiology* 143: 29–36. https://doi.org/10.1148/radiology.143.1.7063747.

Hastings, W. 1970. "Monte Carlo Sampling Methods Using Markov Chains and their Application." *Biometrika* 57: 97–109.

Hermann, R. K., and D. P. Lavender. 1990. "*Pseudotsuga menziesii* (Mirb.) Franco Douglas-fir." In *Silvics of North America: Vol. 1. Conifers. Agriculture Handbook 654*, edited by R. M. Burns and B. H. Honkala, 527–40. Washington DC: USDA Forest Service.

Hijmans, R. J. 2004. *Arc Macro Language (AML) Version 2.1 for Calculating 19 Bioclimatic Predictors*. Berkeley, CA: Museum of Vertebrate Zoology, University of California at Berkeley. http://www.worldclim.org/bioclim.

Iverson, L. R., A. M. Prasad, S. N. Matthews, and M. Peters. 2008. "Estimating Potential Habitat for 134 Eastern US Tree Species under Six Climate Scenarios." *Forest Ecology and Management* 254: 390–406. https://doi.org/10.1016/j.foreco.2007.07.023.

Jones, C. D., J. K. Hughes, N. Bellouin, S. C. Hardiman, G. S. Jones, J. Knight, S. Liddicoat, et al. 2011. "The HadGEM2-ES Implementation of CMIP5 Centennial Simulations." *Geoscientific Model Development* 4: 543–70. https://doi.org/10.5194/gmd-4-543-2011.

Kass, R. E., B. P. Carlin, A. Gelman, and R. M. Neal. 1998. "Markov Chain Monte Carlo in Practice: A Roundtable Discussion." *The American Statistician* 52: 93–100. https://doi.org/10.1080/00031305.1998.10480547.

Kralicek, K. 2023. "kkralicek0/car-sdm: car-sdm (v1.0.1)." Code. Zenodo. https://doi.org/10.5281/zenodo.7586213

Kueppers, L. M., M. A. Snyder, L. C. Sloan, E. S. Zavaleta, and B. Fulfrost. 2005. "Modeled Regional Climate Change and California Endemic Oak Ranges." *Proceedings of the National Academy of Sciences of the United States of America* 45: 16281–6. https://doi.org/10.1073/pnas.0501427102.

Lenihan, J. M., D. Bachelet, R. P. Neilson, and R. Drapek. 2008. "Response of Vegetation Distribution, Ecosystem Productivity, and Fire to Climate Change Scenarios for California." *Climatic Change* 87: 215–30. https://doi.org/10.1007/s10584-007-9362-0.

Lenoir, J., J. C. Gegout, P. A. Marquet, P. de Ruffray, and H. Brisse. 2008. "A Significant Upward Shift in Plant Species Optimum Elevation during the 20th Century." *Science* 320: 1768–71. https://doi.org/10.1126/science.1156831.

Long, J. W., M. K. Anderson, L. Quinn-Davidson, R. W. Goode, F. K. Lake, and C. N. Skinner. 2016. *Restoring California Black Oak Ecosystems to Promote Tribal Values and Wildlife*. General Technical Report PSW-GTR-252. Albany, CA: USDA Forest Service, Pacific Southwest Research Station.

Long, J. W., R. W. Goode, R. J. Gutteriez, J. J. Lackey, and M. K. Anderson. 2017. "Managing California Black Oak for Tribal Ecocultural Restoration." *Journal of Forestry* 115: 426–34. https://doi.org/10.5849/jof.16-033.

Long, J. W., A. Gray, and F. K. Lake. 2018. "Recent Trends in Large Hardwoods in the Pacific Northwest, USA." *Forests* 9: 651. https://doi.org/10.3390/f9100651.

Lutz, J. A., J. W. van Wagtendonk, and J. F. Franklin. 2010. "Climatic Water Deficit, Tree Species Ranges, and Climate Change in Yosemite National Park." *Journal of Biogeography* 37: 936–50. https://doi.org/10.1111/j.1365-2699.2009.02268.x.

Mathys, A. S., N. C. Coops, and R. H. Waring. 2017. "An Ecoregion Assessment of Projected Tree Species Vulnerabilities in Western North America through the 21st Century." *Global Change Biology* 23: 920–32. https://doi.org/10.1111/gcb.13440.

McDonald, P. M. 1990. "*Quercus douglasii* Hook. & Arn. Blue Oak." In *Silvics of North America: Vol. 2. Hardwoods. Agriculture Handbook 654*, edited by R. M. Burns and B. H. Honkala, 631–9. Washington DC: USDA Forest Service.

McKenney, D. W., J. H. Pedlar, K. Lawrence, K. Campbell, and M. F. Hutchinson. 2007. "Potential Impacts of Climate Change on the Distribution of North American Trees." *BioScience* 57: 939–48. https://doi.org/10.1641/B571106.

McNab, W. H., D. T. Cleland, J. A. Freeouf, J. E. Keys, G. J. Nowacki, and C. A. Carpenter. 2007. *Description of Ecological Subregions: Sections of the Conterminous United States*. General Technical Report WO-76B. Washington DC: UDSA Forest Service, Washington Office. https://doi.org/10.2737/WO-GTR-76B.

Metropolis, N., A. Rosenbluth, M. Rosenbluth, A. Teller, and E. Teller. 1953. "Equations of State Calculations by Fast Computing Machines." *The Journal of Chemical Physics* 21: 1087–92. https://doi.org/10.1063/1.1699114.

Moran, P. A. 1950. "Notes on Continuous Stochastic Phenomena." *Biometrika* 37: 17–23.

Mote, P., A. K. Snover, S. Capalbo, S. D. Eigenbrode, P. Glick, J. Littell, R. Raymondi, and S. Reeder. 2014. "Chapter 21: Northwest." In *Climate Change Impacts in the United States: The Third National Climate Assessment*, edited by J. M. Melillo, T. C. Richmond, and G. W. Yohe, 487–513. Washington DC: US Global Change Research Program. https://doi.org/10.7930/J04Q7RWX.

Neelin, J. D., B. Langenbrunner, J. E. Meyerson, A. Hall, and N. Berg. 2013. "California Winter Precipitation Change under Global Warming in the Coupled Model Intercomparison Project Phase 5 Ensemble." *Journal of Climate* 26: 6238–56. https://doi.org/10.1175/JCLI-D-12-00514.1.

Nix, H. A. 1986. "A Biogeographic Analysis of Australian Elapid Snakes." In *Atlas of Elapid Snakes of Australia. Bureau of Flora and Fauna, Australian Flora and Fauna Series 7*, edited by R. Longmore, 4–15. Canberra: Australian Government Publishing Service.

O'Donnell, M. S., and D. A. Ignizio. 2012. *Bioclimatic Predictors for Supporting Ecological Applications in the Conterminous United States*. U.S. Geological Survey Data Series 691. Reston, VA: U.S. Geological Survey.

Pellatt, M. G., S. J. Goring, K. M. Bodtker, and A. J. Cannon. 2012. "Using a Down-Scaled Bioclimate Envelope Model to Determine Long-Term Temporal Connectivity of Garry Oak (*Quercus garryana*) Habitat in Western North America: Implications for Protected Area Planning." *Environmental Management* 49: 802–15. https://doi.org/10.1007/s00267-012-9815-8.

Prasad, A., J. Pedlar, M. Peters, D. McKenney, L. Iverson, S. Matthews, and B. Adams. 2020. "Combining US and Canadian Forest Inventories to Assess Habitat Suitability and Migration Potential of 25 Tree Species under Climate Change." *Diversity and Distributions* 26: 1142–59. https://doi.org/10.1111/ddi.13078.

PRISM Climate Group. 2012. *PRISM Climate Data: Norm81m*. Corvallis, OR: Oregon State University. http://prism.oregonstate.edu.

R Core Team. 2020. *R: A Language and Environment for Statistical Computing*. Vienna: R Foundation for Statistical Computing. https://www.R-project.org/.

Rehfeldt, G. E., B. C. Jaquish, J. López-Upton, C. Sáenz-Romero, J. B. S. Clair, L. P. Leites, and D. G. Joyce. 2014a. "Comparative Genetic Responses to Climate for the Varieties of *Pinus ponderosa* and *Pseudotsuga menziesii*: Realized Climate Niches." *Forest Ecology and Management* 324: 126–37. https://doi.org/10.1016/j.foreco.2014.02.035.

Rehfeldt, G. E., B. C. Jaquish, J. López-Upton, C. Sáenz-Romero, J. B. S. Clair, L. P. Leites, and D. G. Joyce. 2014b. "Comparative Genetic Responses to Climate in the Varieties of *Pinus ponderosa* and *Pseudotsuga menziesii*: Reforestation." *Forest Ecology and Management* 324: 147–57. https://doi.org/10.1016/j.foreco.2014.02.040.

Robert, C., and G. Casella. 2004. "Diagnosing Convergence." In *Monte Carlo Statistical Methods*, Second ed., edited by C. Robert and G. Casella, 459–509. New York: Springer.

Robin, X., N. Turck, A. Hainard, N. Tiberti, F. Lisacek, J. C. Sanchez, and M. Müller. 2011. "pROC: An Open-Source Package for R and S+ to Analyze and Compare ROC Curves." *BMC Bioinformatics* 12: 77. https://doi.org/10.1186/1471-2105-12-77.

Serra-Diaz, J. M., J. Franklin, M. Ninyerola, F. W. Davis, A. D. Syphard, H. M. Regan, and M. Ikegami. 2014. "Bioclimatic Velocity: The Pace of Species Exposure to Climate Change." *Diversity and Distributions* 20: 169–80. https://doi.org/10.1111/ddi.12131.

Smith, W. B., P. D. Miles, C. H. Perry, and S. A. Pugh. 2009. *Forest Resources of the United States 2007: A Technical Document Supporting the Forest Service 2010 RPA Assessment*. General Technical Report WO-78. Washington, DC: Forest Service, Washington Office. 336 pp.

Soja, A. J., N. M. Tchebakova, N. H. F. French, M. D. Flannigan, H. H. Shugart, B. J. Stocks, A. I. Sukhinin, E. I. Parfenova, F. S. Chapin, III, and P. W. Stackhouse, Jr. 2007. "Climate-Induced Boreal Forest Change: Predictions Versus Current Observations." *Global and Planetary Change* 56: 274–96. https://doi.org/10.1016/j.glophlacha.2006.07.028.

Stein, W. I. 1990. "*Quercus garryana* Dougl. Ex Hook. Oregon White Oak." In *Silvics of North America: Vol. 2. Hardwoods. Agriculture Handbook 654*, edited by R. M. Burns and B. H. Honkala, 650–60. Washington DC: USDA Forest Service.

van Vuuren, D. P., J. Edmonds, M. Kainuma, K. Riahi, A. Thomson, K. Hibbard, G. C. Hurtt, et al. 2011. "The Representative Concentration Pathways: An Overview." *Climatic Change* 109: 5–31. https://doi.org/10.1007/s10584-011-0148-z.

Ver Hoef, J. M., D. Johnson, R. Angliss, and M. Higham. 2021. "Species Density Models from Opportunistic Citizen Science Data." *Methods in Ecology and Evolution* 12: 1911–25. https://doi.org/10.1111/2041-210X.13679.

Ver Hoef, J. M., E. E. Peterson, M. B. Hooten, E. M. Hanks, and M.-J. Fortin. 2018. "Spatial Autoregressive Models for Statistical Inference from Ecological Data." *Ecological Monographs* 88: 36–59. https://doi.org/10.1002/ecm.1283.

Wang, T., A. Hamann, D. Spittlehouse, and C. Carroll. 2016. "Locally Downscaled and Spatially Customizable Climate Data for Historical and Future Periods for North America." *PLoS One* 11: e0156720. https://doi.org/10.1371/journal.pone.0156720.

Waring, R. H., and J. F. Franklin. 1979. "Evergreen Coniferous Forests of the Pacific Northwest." *Science* 204: 1380–6. https://doi.org/10.1126/science.204.4400.1380.

Wright, W. J., K. M. Irvine, and M. D. Higgs. 2019. "Identifying Occupancy Model Inadequacies: Can Residuals Separately Assess Detection and Presence?" *Ecology* 100: e02703. https://doi.org/10.1002/ecy.2703.

SUPPORTING INFORMATION

Additional supporting information can be found online in the Supporting Information section at the end of this article.

How to cite this article: Kralicek, Karin, Jay M. Ver Hoef, Tara M. Barrett, and Hailemariam Temesgen. 2023. "Spatial Bayesian Models Project Shifts in Suitable Habitat for Pacific Northwest Tree Species under Climate Change." *Ecosphere* 14(3): e4449. https://doi.org/10.1002/ecs2.4449